ACS Catalysis

pubs.acs.org/acscatalysis Research Article

Zinc Stabilized Azo-anion Radical in Dehydrogenative Synthesis of N-Heterocycles. An Exclusively Ligand Centered Redox Controlled Approach

Siuli Das, Rakesh Mondal, Gargi Chakraborty, Amit Kumar Guin, Abhishek Das, and Nanda D. Paul*

Cite This: *ACS Catal.* 2021, 11, 7498–7512 Read Online

ACCESS | Metrics & More | Article Recommendations | Supporting Information

ABSTRACT: Herein we report an exclusively ligand-centered redox controlled approach for the dehydrogenation of a variety of N-heterocycles using a Zn(II)-stabilized azo-anion radical complex as the catalyst. A simple, easy-to-prepare, and bench-stable Zn(II)-complex (**1b**) featuring the tridentate arylazo pincer, 2-((4-chlorophenyl)diazenyl)-1,10-phenanthroline, in the presence of zinc-dust, undergoes reduction to form the azo-anion radical species $[\mathbf{1b}]^-$ which efficiently dehydrogenates various saturated N-heterocycles such as 1,2,3,4-tetrahydro-2-methylquinoline, 1,2,3,4-tetrahydro-isoquinoline, indoline, 2-phenyl-2,3-dihydro-1*H*-benzoimidazole, 2,3-dihydro-2-phenylquinazolin-4(1*H*)-one, and 1,2,3,4-tetrahydro-2-phenylquinazolines, among others, under air. The catalyst has further been found to be compatible with the cascade synthesis of these N-heterocycles via dehydrogenative coupling of alcohols with other suitable coupling partners under air. Mechanistic investigation reveals that the dehydrogenation reactions proceed via a one-electron hydrogen atom transfer (HAT) pathway where the zinc-stabilized azo-anion radical ligand abstracts the hydrogen atom from the organic substrate(s), and the whole catalytic cycle proceeds via the exclusive involvement of the ligand-centered redox events where the zinc acts only as the template.

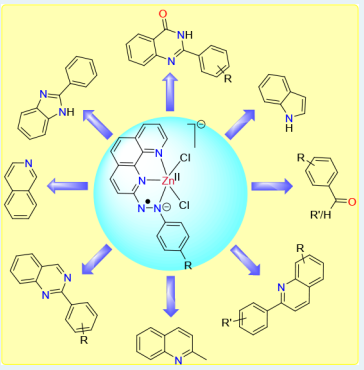

KEYWORDS: *zinc catalyst, azo-anion radical, ligand-centered redox, dehydrogenation, N-heterocycles*

INTRODUCTION

Organic radicals are usually highly reactive in the pure state. However, upon coordination to a transition metal ion, its stability increases significantly.[1] The metal-bound organic radicals are recognized as one of the key intermediates in bringing about radical-type reactions in a controlled manner.[2] In this regard, the synthesis of new transition-metal complexes of redox-active ligands has drawn significant attention in recent years.[2−5] This class of ligands other than coordinating to the metal ions can generate comparatively stable ligand-centered radicals upon selective oxidation and reduction.[3] They can also act as a reservoir of electrons during chemical transformations and hence allow the chemical reactions to proceed under mild conditions avoiding energetically demanding metal-centered redox couples as well as control the substrate binding affinity via selective ligand centered redox processes.[4,5] Over the past decade, significant advances have been made in developing new synthetic strategies utilizing the active participation of transition metal-bound redox-active scaffolds, and various chemical transformations were achieved successfully, which are otherwise difficult or sometimes impossible to accomplish using classical synthetic routes.[2−5]

The catalytic dehydrogenation of N-heterocycles is of significant importance to access heteroarenes which are often found as the structural motifs in various natural products and the pharmaceutical industry.[6] The acceptorless dehydrogenation of N-heterocycles under standard conditions is a thermodynamically uphill process.[7,8] Moreover, the classical transition-metal-catalyzed approaches for the dehydrogenation of N-heterocycles proceed via the formation of metal-hydride intermediates involving energetically demanding two-electron metal-centered redox events. As a consequence, these reactions almost always require harsh reaction conditions.[8−11] Several heterogeneous catalysts based on noble metal and transition metal oxides have been reported for dehydrogenation of N-heterocycles.[9] However, most of these catalytic systems require high temperature and showed limited functional group tolerance. On the other hand, only a few homogeneous catalysts are reported for these reactions (Scheme 1). After the pioneering work by Yamagushi and Fujita[10a] on Ir-catalyzed dehydrogenation of tetrahydroquinoline derivatives, a few more Ir-catalyzed dehydrogenation reactions have been reported by Xiao,[10b] Huang,[10c] Crabtree,[10d] Albrecht,[10e] and others.[10f,g] Despite significant advances, the use of expensive

Received: January 20, 2021
Revised: May 26, 2021
Published: June 9, 2021

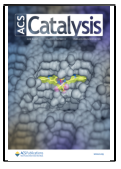

https://doi.org/10.1021/acscatal.1c00275
ACS Catal. 2021, 11, 7498–7512

Scheme 1. A Brief Survey of Previous Works and Schematic Representation of Our Present Work.[10a,b,d,e,11a,b,12b]

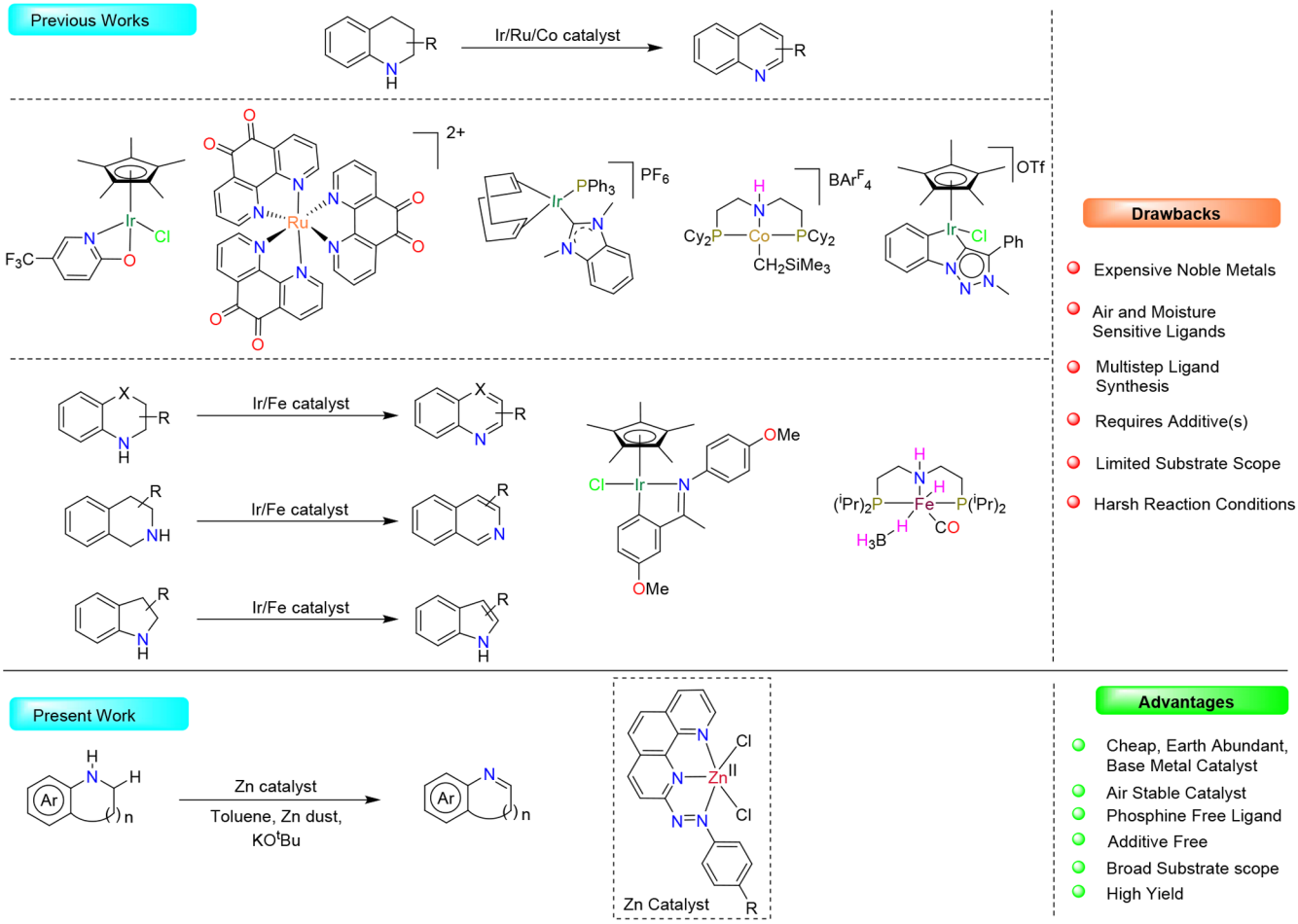

and relatively scarce iridium catalysts may limit the applications of these methods. The use of inexpensive, earth-abundant, and environmentally benign 3d-base metals for these reactions would be beneficial in terms of sustainability and scalability. In this regard, the work by Jones and co-workers on the Fe and Co-catalyzed dehydrogenation of N-heterocycles is worthy to mention.[11] However, the use of an air-sensitive phosphine-based ligand limits the application of these methods to some extent. In 2014, Stahl and co-workers reported the dehydrogenation of N-heterocycles under air using a bifunctional quinone catalyst.[12] Therefore, the development of alternative synthetic strategies for the dehydrogenation of N-heterocycles under comparatively mild conditions is desirable.

Herein we report a simple strategy for the dehydrogenation reactions utilizing a metal(zinc)-stabilized azo-anion radical ligand. A well-defined Zn(II)-complex ([**1b**]$^-$) featuring a one-electron reduced 2-((4-chlorophenyl)diazenyl)-1,10-phenanthroline ligand shows good activity in the dehydrogenation of a wide variety of N-heterocycles such as 1,2,3,4-tetrahydro-2-methyl quinoline, 1,2,3,4-tetrahydroisoquinoline, indoline, 2-phenyl-2,3-dihydro-1*H*-benzimidazole, 2,3-dihydro-2-phenyl-quinazolin-4(1*H*)-one, and 1,2,3,4-tetrahydro-2-phenylquinazolines. The catalyst [**1b**]$^-$ has further been found to be compatible with the cascade synthesis of these N-heterocycles via dehydrogenative coupling of alcohols with other suitable coupling partners under air.[13] Mechanistic investigation reveals that the dehydrogenation reactions proceed via a one-electron hydrogen atom transfer (HAT) pathway where the zinc-stabilized azo-anion radical ligand abstracts the hydrogen atom from the organic substrate(s), and the whole catalytic cycle proceeds via the exclusive involvement of the ligand-centered redox events where the zinc acts only as the template.

RESULT AND DISCUSSION

Synthesis and Characterization of the Catalysts. Our present work begins with the synthesis of two new well-defined Zn(II)-complexes **1a** and **1b** featuring the redox noninnocent tridentate pincers, 2-(phenyldiazenyl)-1,10-phenanthroline (**L**^{1a}) and 2-((4-chlorophenyl)diazenyl)-1,10-phenanthroline (**L**^{1b}), respectively. The reaction of **L**^{1a,1b} with an equimolar amount of $ZnCl_2$ in ethanol at room temperature under air yielded two new orange-colored complexes [Zn(L^{1a})Cl$_2$] (**1a**) and [Zn(L^{1b})Cl$_2$] (**1b**) in 93 and 94% yields, respectively (Scheme 2). The elemental analysis supports their formulations. Both the complexes are diamagnetic. Well-resolved ^{1}H NMR spectra were obtained in the range 7.6−9.5 ppm (see SI). X-ray structure of **1b** reveals a penta-coordinate geometry around the Zn(II)-ion (Figure 1). The pincer ligand, **L**^{1b}, coordinates the Zn(II)-center in a tridentate fashion, and two chlorido ligands occupy the rest of the two coordination sites. The two N-donor atoms N1(phen) and N4(azo) occupy the apical positions with an N1−Zn−N4 angle of 143.60(6)° with a calculated τ value of 0.24.[14] The N−N bond distance was

https://doi.org/10.1021/acscatal.1c00275
ACS Catal. 2021, 11, 7498−7512

Scheme 2. Synthesis of the Zn(II)-Complexes 1a and 1b

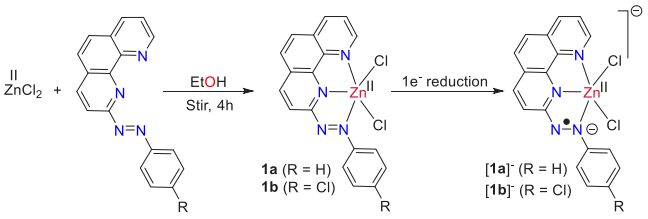

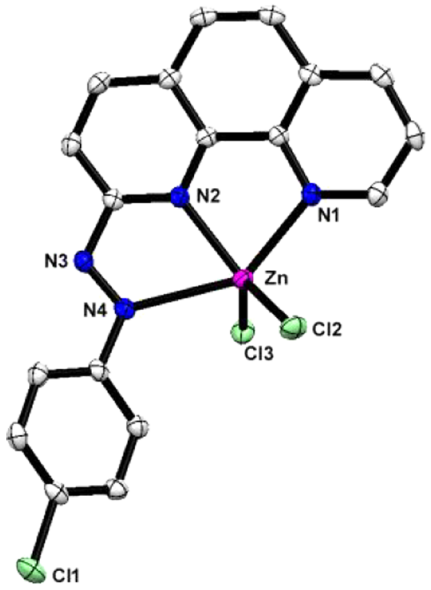

Figure 1. ORTEP view of $[ZnL^{1b}Cl_2]$ (**1b**) with ellipsoids at the 50% probability level. Hydrogen atoms are omitted for clarity.

found to be 1.246(2)Å, indicating the presence of unreduced azo-chromophore.[15,16]

The complexes **1a** and **1b** undergo one single-electron reversible reduction in the potential range between −0.17 and −0.19 V, and one irreversible reduction in the potential range between −1.07 and −1.09 V, in acetonitrile/0.1 M Et_4NClO_4 using platinum as working electrode, and saturated Ag/AgCl as the reference electrode (see SI for details). The cyclic voltammogram of **1b** is displayed in Figure 2, and the corresponding electrochemical data are submitted in SI. Zn(II) being the redox-inactive center, the redox responses are expected because of the ligand-centered reduction (Figure 2). The EPR spectrum of the electrogenerated species obtained after exhaustive electrolysis of **1b** at −0.5 V showed a single line isotropic spectrum with minor hyperfine coupling at g_{iso} = 1.9737, indicating the formation of a ligand-centered radical upon one-electron reduction (Figure 3).[15,16] Isotropic

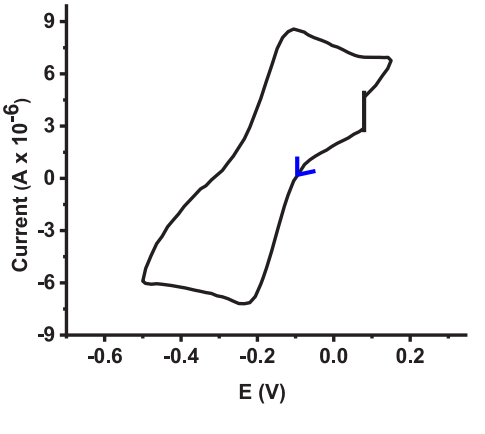

Figure 2. Cyclic voltammogram of **1b** in acetonitrile/0.1 M Et_4NClO_4 using platinum as working electrode, platinum wire as auxiliary electrode, and saturated Ag/AgCl as reference electrode. Scan rate = 100 mV s^{-1}.

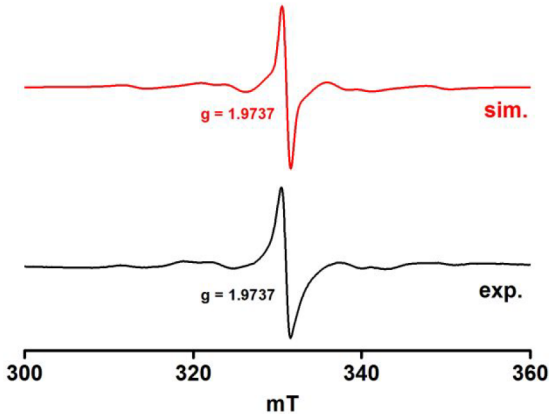

Figure 3. X-band EPR spectrum of $[\mathbf{1b}]^-$ in dichloromethane at 77K.

simulation of the experimental spectrum indeed is in agreement with the ligand-centered EPR spectrum with hyperfine interaction with ^{14}N (I = 1) nuclei. It is worth mentioning here that the experimental spectrum (along with hyperfine) simulation requires consideration of three species: one with hyperfine for 1 N, another for 2 N with a slightly different A value, and the third one without nitrogen hyperfine. This may be because the radical can delocalize into the aromatic ring of the arylazo scaffold which has been substantiated by the DFT studies. The experimental and simulated EPR spectra are displayed in Figure 3, and the simulation parameters are shown in SI. Notably, these complexes in the presence of zinc dust and KO^tBu also undergo one-electron reduction to form the azo-anion radical species $[\mathbf{1a/1b}]^-$. We tried to isolate and grow the single crystals of the one-electron reduced species $[\mathbf{1a/b}]^-$. However, after repeated trials, we could not obtain the single crystals suitable for X-ray diffraction.

Electronic structure elucidation using DFT at the B3LYP level revealed that the complex, $Zn(L^{1b})Cl_2$ (**1b**), is a closed-shell singlet species. Molecular orbital analysis showed that the LUMOs are ligand-centered; primarily localized on the azo-chromophore. On the other hand, the one-electron reduced complex, $[Zn(L^{1b})Cl_2]^-$ ($[\mathbf{1b}]^-$), was found to be an open-shell doublet species with a spin population of +0.003 on the Zn(II)-center and −0.997 spin population on the azo-aromatic scaffold (Figure 4).

Catalysis. Catalytic Dehydrogenation of N-Heterocycles. With the characterization data of **1a** and **1b** in hand, we envisaged that a one-electron reduced azo-anion radical ligand coordinated to Zn(II)-ion in $[\mathbf{1a}]^-$ and $[\mathbf{1b}]^-$ would abstract the hydrogen atom from various organic substrates (N-heterocycles) leading to efficient dehydrogenation reactions. To begin with, initially, we studied the monodehydrogenation reactions where the removal of two hydrogen atoms (one from N−H and one from C−H) from the saturated N-heterocycles would produce the desired N-heterocycles. We chose 2,3-

https://doi.org/10.1021/acscatal.1c00275
ACS Catal. 2021, 11, 7498−7512

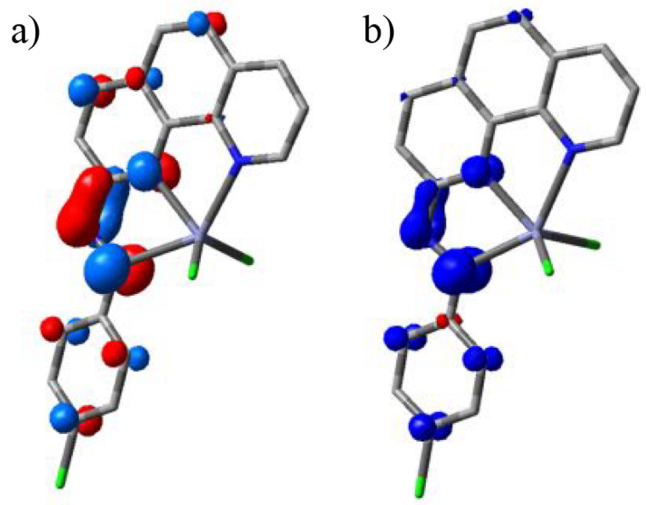

Figure 4. (a) LUMO of **1b**. (b) Spin density plot of $[\mathbf{1b}]^-$.

dihydro-2-phenylquinazolin-4(1*H*)-one (**2a**) as the model substrate to find out the optimal reaction parameters. Optimization of the reaction conditions reveals that the dehydrogenation of **2a** proceeds best in the presence of 4.0 mol % of **1b**, 0.5 equiv of KO^{t}Bu, 0.5 equiv of Zn dust under air at 100 °C (Table 1). Catalyst **1b** was found to be more effective as compared to catalyst **1a**. A maximum yield of 96% was obtained under the optimal conditions using **1b** as the catalyst (Table 1, entry 12). Among the different bases and solvents used during dehydrogenation reactions, KO^{t}Bu and toluene, respectively, were found to be most effective (see Table 1 for details). The catalytic dehydrogenation did not proceed under an argon atmosphere (Table 1, entry 15). A quantitative conversion was observed when one equivalent of **2a** was subjected to dehydrogenation in the presence of one equivalent of the catalyst under an argon atmosphere. However, under a pure oxygen environment, we did not observe any significant improvement of yield (Table 1, entry 16).

Control experiments revealed that the reaction did not proceed well in the absence of a base (Table 1, entry 17). In the presence of only KO^{t}Bu, **3a** was obtained in 19% yields (Table 1, entry 18). In the presence of $ZnCl_2$ or $\mathbf{L}^{1b}$, **3a** was obtained in 20 and 19% yields, respectively (Table 1, entries 19, 20). Instead of **1b**, when a 1:1 mixture of $ZnCl_2$ and $\mathbf{L}^{1b}$ was used as catalyst, **3a** was obtained in 43% yields (Table 1, entry 21). This slight increase of yield may be due to the in situ formation of some amount of the catalyst **1b**. The reaction did not proceed at all in the presence of only zinc dust (Table 1, entry 22). No noticeable increase in yields was observed on varying the catalyst loading or any other reaction parameters such as base, solvent, or temperature beyond the optimal conditions.

We screened the substrate scope for a variety of multi-substituted 2,3-dihydro-2-phenylquinazolin-4(1*H*)-ones. The present strategy is compatible with various 2,3-dihydro-2-phenylquinazolin-4(1*H*)-ones bearing both electron-donating

Table 1. Optimization of the Reaction Conditions for Dehydrogenation of 2,3-Dihydro-2-phenylquinazolin-4(1*H*)-one (2a)[a,b,c,d]

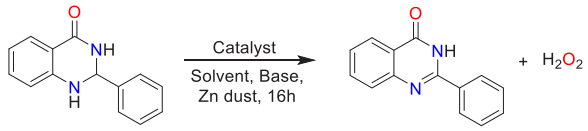

entry	catalyst (mol %)	solvent	base	temperature (°C)	yield[b] (%)
1	**1b** (7 mol %)	toluene	KO^{t}Bu (0.7 equiv)	120	96
2	**1b** (7 mol %)	toluene	KO^{t}Bu (0.7 equiv)	100	96
3	**1b** (7 mol %)	xylene	KO^{t}Bu (0.7 equiv)	100	95
4	**1b** (7 mol %)	THF	KO^{t}Bu (0.7 equiv)	100	73
5	**1b** (7 mol %)	ACN	KO^{t}Bu (0.7 equiv)	100	trace
6	**1b** (7 mol %)	ethanol	KO^{t}Bu (0.7 equiv)	100	trace
7	**1b** (7 mol %)	toluene	NaO^{t}Bu (0.7 equiv)	100	94
8	**1b** (7 mol %)	toluene	KOH (0.7 equiv)	100	92
9	**1b** (7 mol %)	toluene	NaOH (0.7 equiv)	100	91
10	**1b** (7 mol %)	toluene	K_3PO_4(0.5 equiv)	100	32
11	**1b** (7 mol %)	toluene	KO^{t}Bu (0.5 equiv)	100	96
12	**1b** (4 mol %)	toluene	KO^{t}Bu (0.5 equiv)	100	96
13	**1b** (3 mol %)	toluene	KO^{t}Bu (0.5 equiv)	100	94
14	**1a** (4 mol %)	toluene	KO^{t}Bu (0.5 equiv)	100	92
15[c]	**1b** (5 mol %)	toluene	KO^{t}Bu (0.5 equiv)	100	trace
16[d]	**1b** (4 mol %)	toluene	KO^{t}Bu (0.5 equiv)	100	96
17	**1b** (4 mol %)	toluene	-	100	trace
18	-	toluene	KO^{t}Bu (0.5 equiv)	100	19
19	$ZnCl_2$ (5 mol %)	toluene	KO^{t}Bu (0.5 equiv)	100	20
20	$\mathbf{L}^{1a,b}$ (4.0 mol %)	toluene	KO^{t}Bu (0.5 equiv)	100	19
21	$ZnCl_2$+L^{1b} (1:1) (5 mol %)	toluene	KO^{t}Bu (0.5 equiv)	100	43
22	Zn-dust	toluene	KO^{t}Bu (0.5 equiv)	100	NR

[a]Stoichiometry: **2a** (1.0 mmol), Zn-dust (0.5 equiv). [b]Isolated yields after column chromatography. [c]Under argon atmosphere. [d]Under pure oxygen atmosphere.

https://doi.org/10.1021/acscatal.1c00275
ACS Catal. 2021, 11, 7498−7512

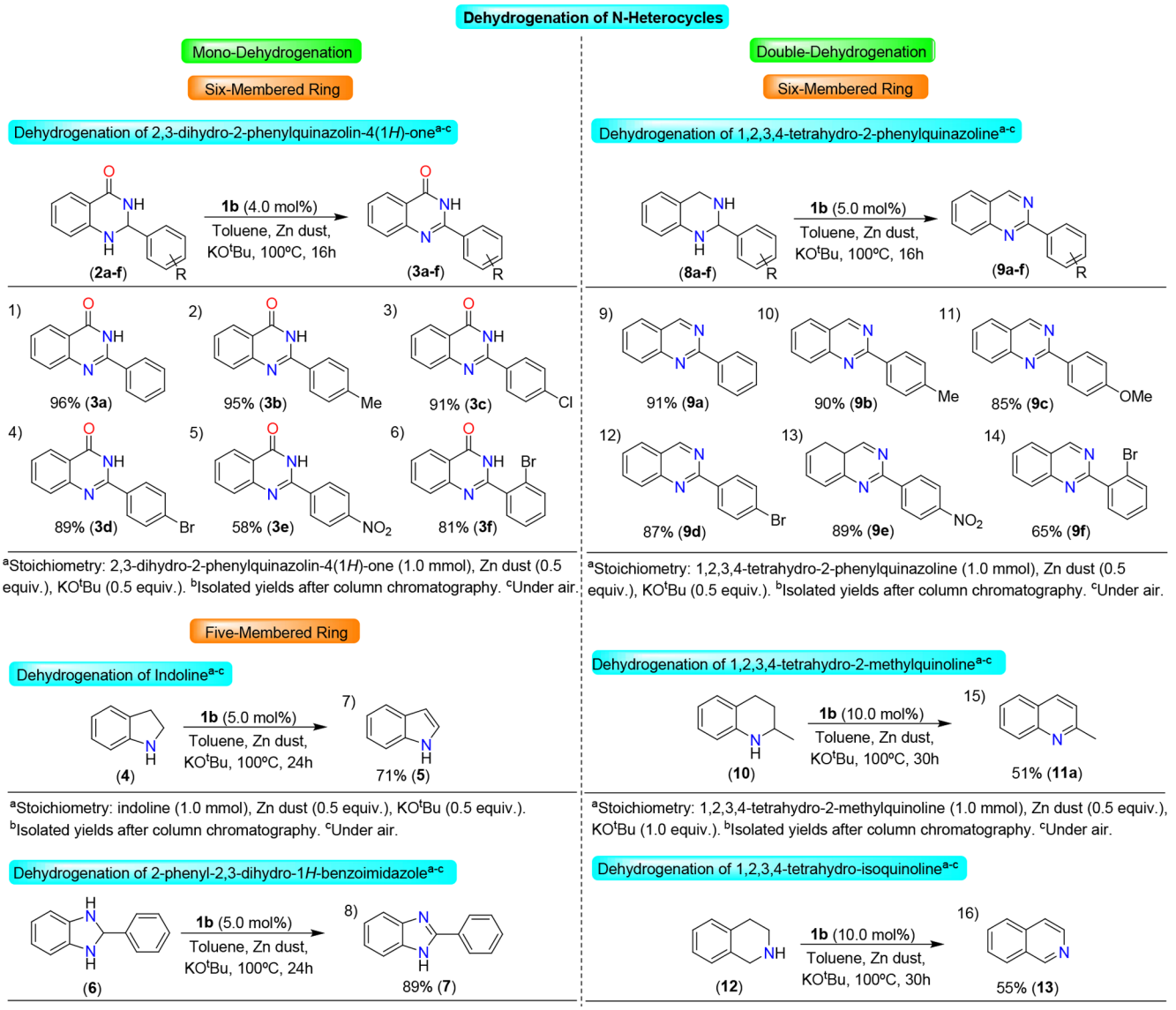

Figure 5. Dehydrogenation of various saturated N-heterocycles using **1b** as catalyst.

and -withdrawing substituents at the different positions of the phenyl ring. The corresponding substituted 2-phenylquinazolin-4(1*H*)-ones (**3a−f**) were obtained in moderate to good isolated yields (Figure 5, entries 1−6). Five-membered N-heterocycles, such as indoline (**4**), and 2-phenyl-2,3-dihydro-1*H*-benzoimidazole (**6**), also undergo dehydrogenation to produce **5** and **7** in 71 and 89% yields, respectively (Figure 5, entries 7 and 8).

We also studied the double dehydrogenation reactions with a few chosen N-heterocycles. Dehydrogenation of 1,2,3,4-tetrahydro-2-phenylquinazoline (**8a**) proceeds smoothly under the optimized conditions used during monodehydrogenation reactions (Figure 5, entry 9); only slightly higher catalyst loading 5.0 mol % is required. Different substituted 1,2,3,4-tetrahydro-2-phenylquinazolines (**8b−f**) undergo dehydrogenation to afford the respective 2-phenylquinazolines (**9b−f**) in moderate to good isolated yields (Figure 5, entries 10−14). More difficult substrates such as 1,2,3,4-tetrahydro-2-methylquinoline (**10**) and 1,2,3,4-tetrahydro-isoquinoline (**12**) were also found to be compatible for dehydrogenation to yield 2-methylquinoline (**11a**) and isoquinoline (**13**) in 51 and 55% isolated yields, respectively, under the optimal conditions with a slightly higher catalyst loading of 10.0 mol % (Figure 5, entries 15 and 16). It is worth mentioning that with low-yielding reactions other than the desired products, we observe unreacted starting materials during chromatographic purification. However, we did not notice any side products.

One-Pot Cascade Synthesis of N-Heterocycles via Dehydrogenative Coupling. Dehydrogenative coupling of alcohols with suitable coupling partners offers an attractive eco-friendly approach for the construction of various N-heterocycles from cheap and earth-abundant raw materials.[13,17−20] Since our Zn-catalyst, **1b**, showed promising results during the dehydrogenation of preformed saturated N-heterocycles, we decided to check the viability of the one-pot cascade synthesis of a few selected N-heterocycles such as 2-arylquinazolin-4(3*H*)-ones,[18] 2-arylquinazolines,[19] and quinolines[20] via dehydrogenative functionalization of alcohols. A wide variety of 2-arylquinazolin-4(1*H*)-ones and 2-arylquinazolines were prepared via dehydrogenative coupling of alcohols with 2-aminobenzamides and 2-aminobenzylamines, respectively. However, quinolines were prepared via dehydrogenative

https://doi.org/10.1021/acscatal.1c00275
ACS Catal. 2021, 11, 7498−7512

Table 2. Substrate Scope for the Dehydrogenative Coupling of Benzyl Alcohols and 2-Aminobenzamides to Various Substituted Quinazolin-4(3*H*)-ones[a,b,c]

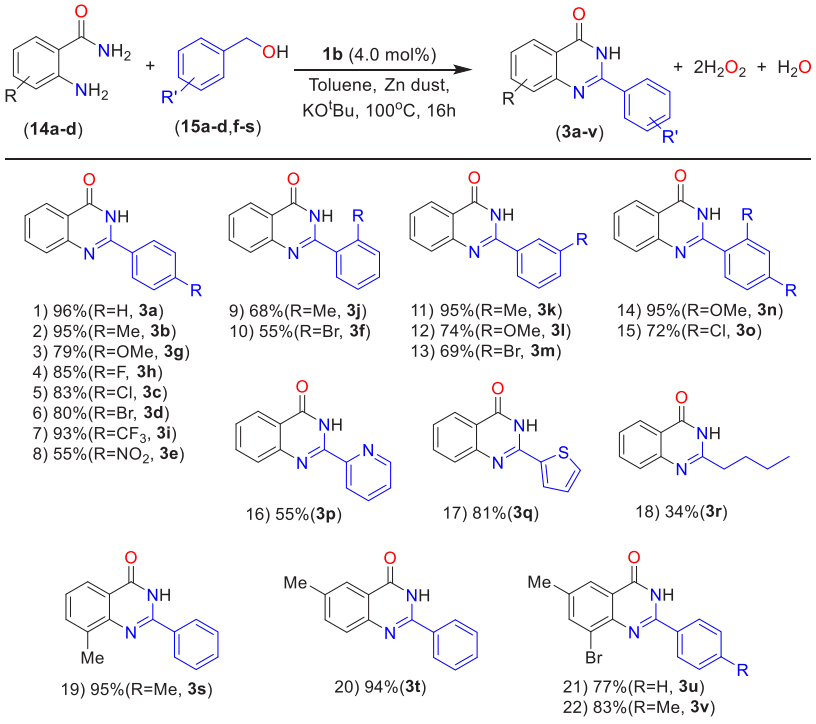

[a]Stoichiometry: 2-aminobenzamide (1.0 mmol); benzyl alcohol (1.1 mmol); Zn dust (0.5 equiv), KO^{t}Bu (0.5 equiv). [b]Isolated yields after column chromatography. [c]Under air.

Table 3. Substrate Scope for the Dehydrogenative Coupling of Benzyl Alcohols and 2-Aminobenzylamines to Various Substituted Quinazolines[a,b,c]

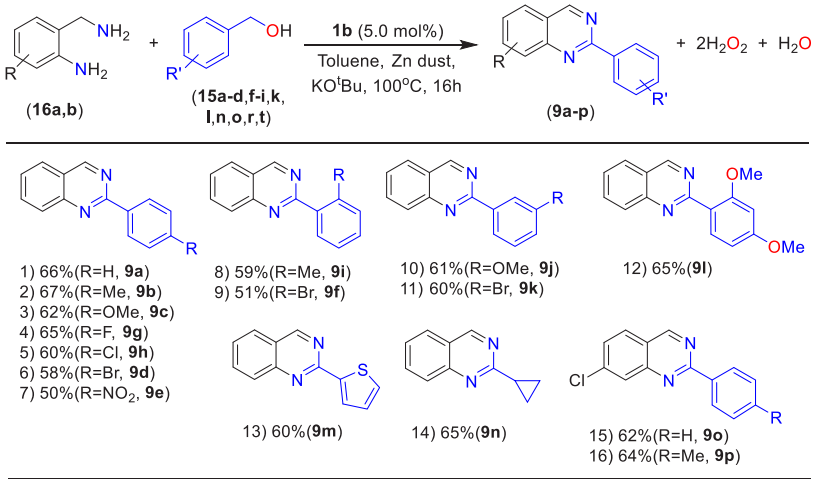

[a]Stoichiometry: 2-aminobenzylamine (1.0 mmol); benzyl alcohol (1.1 mmol); Zn dust (0.5 equiv), KO^{t}Bu (0.5 equiv). [b]Isolated yields after column chromatography. [c]Under air.

coupling of alcohols with ketones bearing an active methylene group.

Various reaction conditions were screened to get the optimal conditions for these dehydrogenative coupling reactions (Table S5, entries 1−19). Best results for 2-phenylquinazolin-4(3*H*)-one (**3a**) and 2-phenylquinazoline (**9a**) were obtained on carrying out the reactions in toluene at 100 °C for 16 h in the presence of 0.5 equiv of Zn dust, 0.5 equiv. KO^{t}Bu and 5.0 mol % **1b** under air. The maximum isolated yields of **3a** and **9a** obtained under the optimal conditions are 96 and 66%, respectively (Table S5, entry 8). Additionally, the dehydrogenative coupling of benzyl alcohol and ketone proceeds at 90 °C to produce a maximum yield of 96% of 2-phenylquinoline (**11b**) in just 10 h with 1.0 mol % catalyst (**1b**) loading in the presence of 0.3 equiv. KO^{t}Bu and 0.4 equiv of Zn dust under air (Table S5, entry 3, see SI for details).

Substrate scope was explored to check the versatility of the **1b**-catalyzed dehydrogenative coupling reactions. The catalyst

https://doi.org/10.1021/acscatal.1c00275
ACS Catal. 2021, 11, 7498−7512

Table 4. Substrate Scope for the Dehydrogenative Coupling of Ketones and 2-Aminobenzylalcohols to Various Substituted Quinolines[a,b,c]

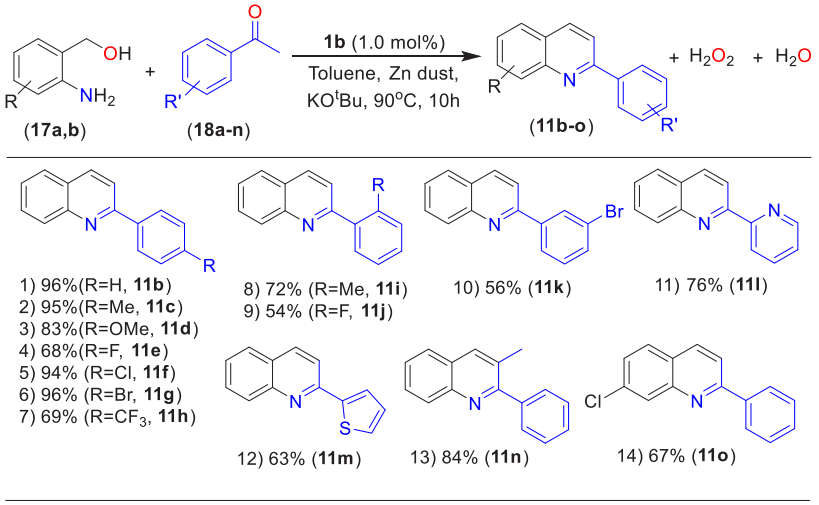

[a]Stoichiometry: acetophenone (1.1 mmol); 2-aminobenzyl alcohol (1.0 mmol); Zn dust (0.4 equiv), KO^{t}Bu (0.3 equiv). [b]Isolated yields after column chromatography. [c]Under air.

Scheme 3. Control Experiments to Probe the Active Involvement of $[1b]^-$ during Dehydrogenation and Dehydrogenative Coupling Reactions[a]

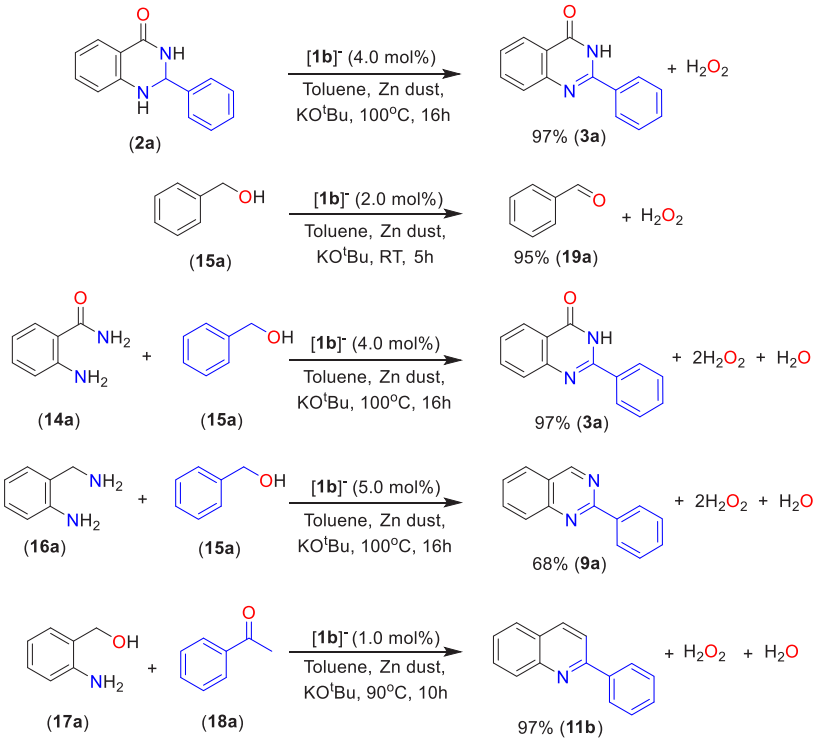

[a]All the above reactions were performed under air.

1b is well tolerant toward a wide variety of substituted benzyl alcohols and ketones bearing electron-donating, -withdrawing, and heteroaryl functionalities. Irrespective of the position (*-ortho*, *-meta*, or *-para*) of the electron-donating substituents such as -Me, - OMe, on the phenyl ring of benzyl alcohols, the desired quinazolin-4(3*H*)-ones, **3b**, **3g**, **3j**, **3k**, **3l**, and **3n** were isolated in 68−95% yields (Table 2, entries 2, 3, 9, 11, 12, and 14). While the respective quinazolines **9b**, **9c**, **9i**, **9j**, and **9l** were obtained in 59−67% isolated yields (Table 3, entries 2, 3, 8, 10, 12). Electron-withdrawing halogens also survived during the catalytic reaction to produce the corresponding quinazolin-4(3*H*)-ones, **3c**, **3d**, **3f**, **3h**, **3m**, **3o** in 55−85% (Table 2, entries 4−6, 10, 13, 15) and quinazolines **9d**, **9f**, **9g**, **9h**, and **9k** in 51−65% isolated yields (Table 3, entries 4−6, 9, 11). Reactions also proceed well in the presence of $-CF_3$ and $-NO_2$ groups to produce the corresponding quinazolin-4(3*H*)-ones, **3e** and **3i**, in 55 and 93% yields, respectively (Table 2, entries 7 and 8). Under identical conditions, 2-(4-

https://doi.org/10.1021/acscatal.1c00275
ACS Catal. 2021, 11, 7498−7512

Scheme 4. (1)Trapping of (Ketyl)-Radical-TEMPO Adduct during [1b]$^-$ Catalyzed Dehydrogenation of 2a and 15a and TEMPO Bound [1b]$^-$ by HRMS. (2) Dehydrogenation of Cyclobutanol

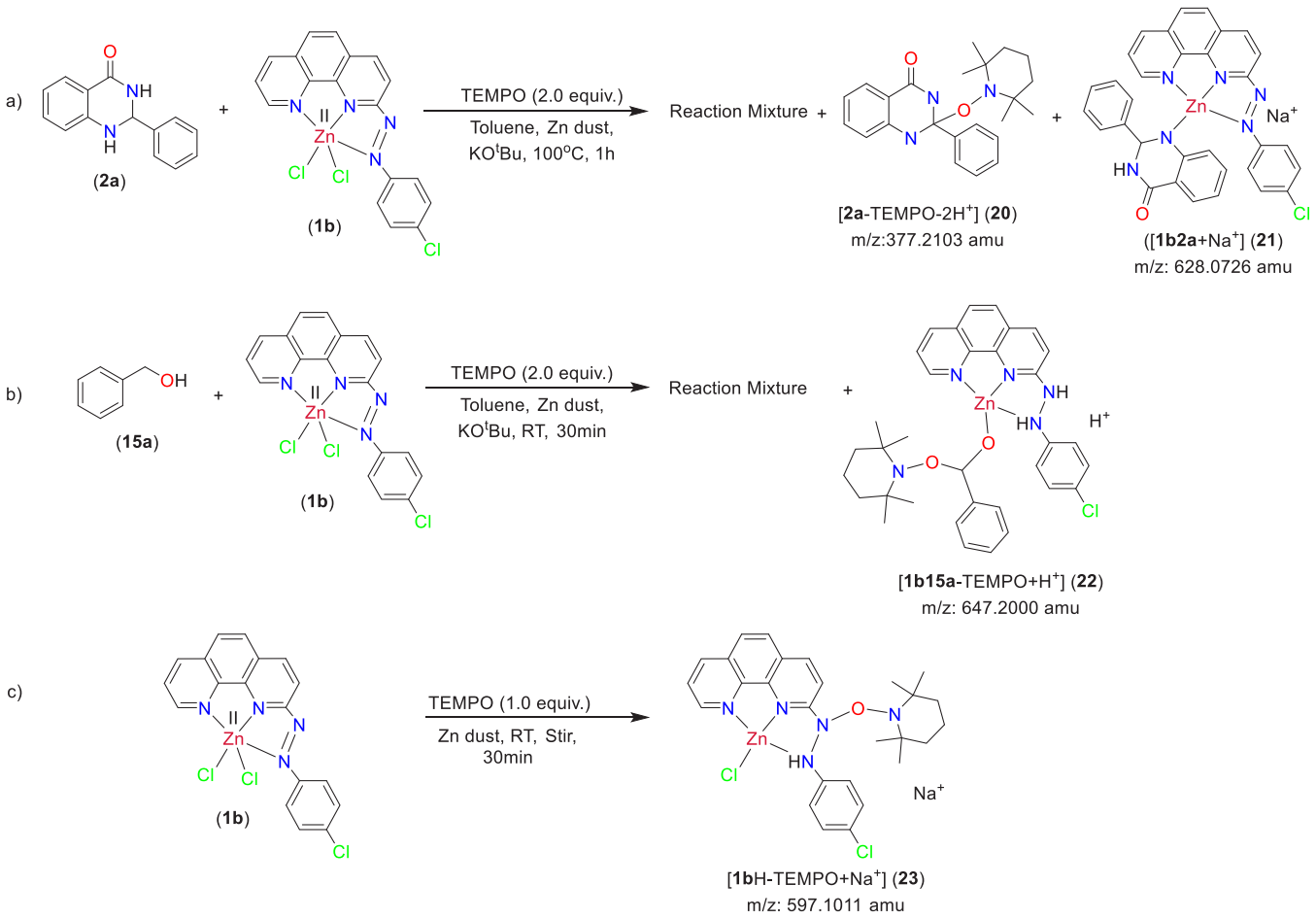

nitrophenyl)quinazoline, **9e** was obtained in 50% yield (Table 3, entry 7). With heteroaryl alcohols, the corresponding quinazolin-4(3*H*)-ones, **3p**, **3q**, and quinazoline **9m** were isolated in 55, 81, and 60% isolated yields, respectively (Table 2, entries 16 and 17, Table 3, entry 13). Reaction with pentan-1-ol (**15r**) produced the corresponding quinazolin-4(3*H*)-one, **3r**, in 34% isolated yield (Table 2, entry 18) while cyclopropyl methanol afforded the corresponding quinazoline, **9n** in 65% isolated yield (Table 3, entry 14). Reactions also proceed well with a variety of 2-aminobenzamides and 2-aminobenzylamines containing both electron-donating and -withdrawing groups. The corresponding quinazolin-4(3*H*)-ones (**3s**−**3v**, Table 2, entries 19−22) and quinazolines (**9o**, **9p**, Table 3, entries 15, 16) were obtained in moderate to good isolated yields.

Substrate scope was also explored for the synthesis of quinolines. Acetophenones having electron-donating −Me and −OMe groups at *para*-position produced the corresponding quinolines in 95 and 83% isolated yields, respectively (Table 4, entries 2, 3). Reactions proceed efficiently with electron-withdrawing halogens as well as with strong electron-withdrawing groups like $-CF_3$ to produce the corresponding quinolines (**11e**-**11h**) in 68−96% yields (Table 4, entries 4−7). Heteroaryl and nonmethyl ketones were also found to be compatible under the optimal reaction conditions yielding the respective quinolines **11l**, **11m**, and **11n** in 76, 63, and 84% yields, respectively (Table 4, entries 11−13). Quinolines were also obtained in satisfactory yield with substituted 2-aminobenzyl alcohol (Table 4, entry 14).

Mechanistic Investigation. We performed a set of control experiments to understand and unveil the reaction mechanism. The catalyst **1b** undergoes reduction in the presence of Zn-dust to form the one-electron reduced Zn(II)-stabilized azo-anion radical species [**1b**]$^-$ (see above). To probe the involvement of [**1b**]$^-$, the substrates **2a** and **15a** were subjected to dehydrogenation using the preformed [**1b**]$^-$ as

https://doi.org/10.1021/acscatal.1c00275
ACS Catal. 2021, 11, 7498−7512

the catalyst. As expected, the dehydrogenation reactions proceed smoothly under the optimized conditions, and the corresponding dehydrogenated products were isolated in 97 and 95% yields, respectively (Scheme 3). $[\mathbf{1b}]^-$ was further found to be equally efficient during the synthesis of 2-phenyl quinazolin-4(3*H*)-one (**3a**), quinazoline (**9a**), and quinoline (**11b**) via dehydrogenative coupling reactions (Scheme 3).

Once the active involvement of the Zn(II)-stabilized azo-anion radical species $[\mathbf{1b}]^-$ is affirmed in the above dehydrogenative reactions, we performed the dehydrogenation of **2a** and **15a** under the optimized conditions in the presence of a radical inhibitor like TEMPO. The dehydrogenation reactions did not proceed at all in the presence of TEMPO; instead, investigation of the reaction mixture using HRMS indicates the formation of adducts like **2a−TEMPO** (**20**), **1b2a** (**21**), and **1b15a−TEMPO** (**22**) (Scheme 4, (1a), (1b); see SI for details). The preformed $[\mathbf{1b}]^-$ also reacts with TEMPO. HRMS analysis of the reaction mixture of TEMPO and in situ formed $[\mathbf{1b}]^-$ showed an intense peak at 597.1011 amu, indicating the formation of [**1bH−TEMPO**] (**23**) adduct (Scheme 4, (1c)). To further substantiate the involvement of organic radical and to differentiate between two-electron hydride transfer and one-electron hydrogen atom transfer (HAT) pathways, the radical-clock substrate cyclobutanol was subjected to dehydrogenation under the optimal conditions. The formation of multiple ring cleavage products is indeed in accordance with the one-electron hydrogen atom transfer (HAT) pathway involving the ketyl radical intermediate (Scheme 4, (2), and SI Figure 125).[21] A kinetic isotope effect (KIE) experiment was also carried out to have a better understanding of the $[\mathbf{1b}]^-$ catalyzed dehydrogenation reactions (Scheme 5). Under the optimized conditions, dehydrogenation of **15a-D** exhibited a KIE value of ∼14, which is in agreement with similar HAT processes involving ligand-centered radicals.[4g,22]

Scheme 5. Kinetic Isotope Effect Study

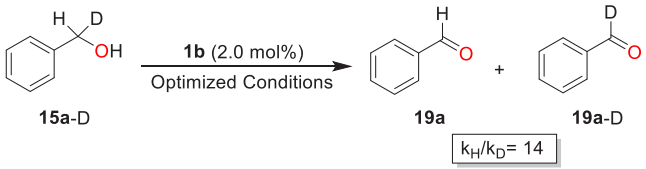

In catalyst **1b**, since Zn(II) is redox inactive while the aryl-azo scaffold is redox-active and undergoes reduction to form azo-anion radical, we performed a few control experiments to investigate the involvement of the aryl-azo scaffold. Stoichiometric reaction was carried out using **1b**, and 1-phenyl ethanol (**15e**) under the optimal conditions in the presence of argon. IR spectroscopic analysis of the reaction mixture revealed the N−H stretching at 3030 and 3063 cm^{-1} (Figure 6; see SI for details), indicating the active participation of the azo-chromophore during the dehydrogenation of alcohols.[15,16,22,23] N−N single bond stretching was observed at 1300 cm^{-1}.[23] Deuterium labeling experiment using deuterated 1-phenyl ethanol showed the N−D stretching at 2084 and 2120 cm^{-1}, which further confirms the involvement of the coordinated aryl-azo scaffold (Figure 6).

To investigate the fate of the abstracted hydrogen atom, an intermolecular hydrogen transfer reaction was performed with 4-methoxy benzaldehyde (**19e**). Maintaining a closed system

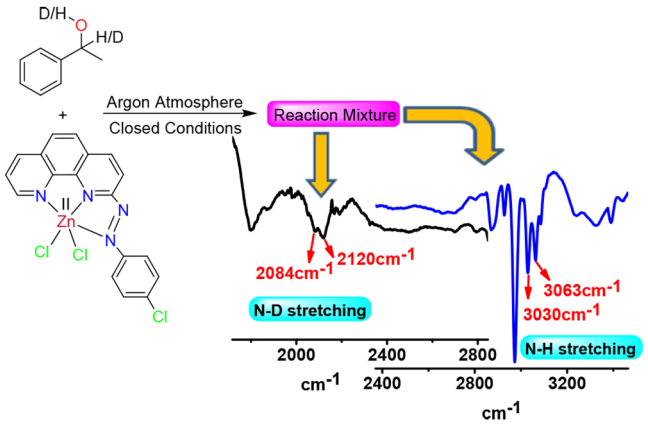

Figure 6. IR spectra of reaction mixture showing N−H and N−D stretching.

under both argon atmosphere and air, when dehydrogenation of 1-phenyl ethanol (**15e**) was carried out separately in the presence of **19e**, no hydrogenated product of the corresponding aldehyde (**19e**) was obtained (see SI Scheme S1). Instead spectroscopic investigation of the reaction mixture reveals the formation of H_2O_2 (Figure 7).[15,16] We also have quantified the

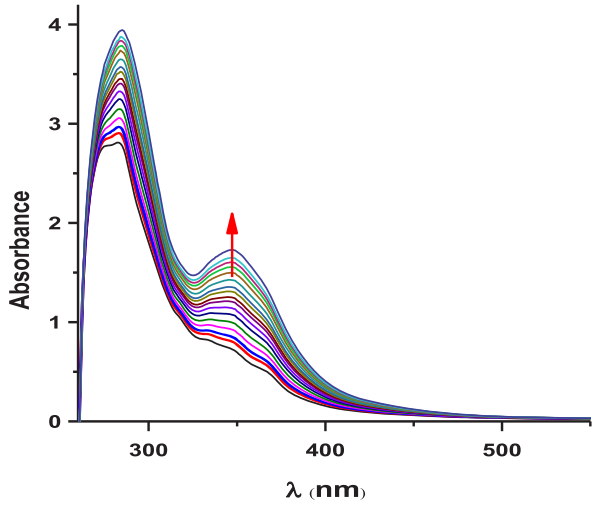

Figure 7. Detection of H_2O_2. Absorption spectral changes during formation of I_3^- in prescence of H_2O_2.

amount of H_2O_2 formed during the dehydrogenation of benzyl alcohol (**15a**). After 2 h of the reaction, under the optimized conditions, 0.69 equiv of H_2O_2 was obtained, while after the completion of the reaction after 5 h, we obtained 0.83 equiv of H_2O_2 from the reaction mixture. Compared with the yield of benzaldehyde after 5 h, it seems that the H_2O_2 formed during the reaction decomposes under our experimental conditions (see SI). Next, **2a** was subjected to dehydrogenation in the presence of H_2O_2 to check the background reaction. Under the optimized conditions in the presence of 1.0 equiv of H_2O_2, **3a** was obtained in 18% yield, which is identical to the yield obtained in the presence of only KO^{t}Bu (Table 1, entry 18), indicating the noninvolvement of H_2O_2 during the dehydrogenation reactions.

To get a deeper insight into the reaction mechanism, kinetic studies were carried out using 1-phenyl ethanol (**15e**) as the model substrate.[16] Under pseudo-first-order conditions, k_{obs}

https://doi.org/10.1021/acscatal.1c00275
ACS Catal. 2021, 11, 7498−7512

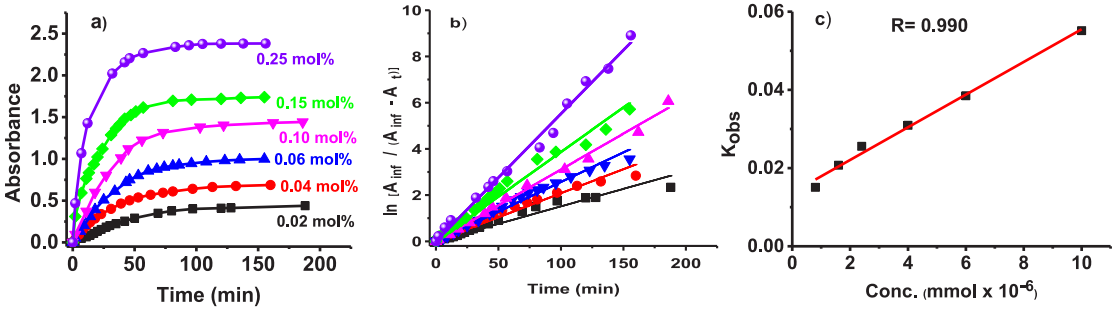

Figure 8. Pseudo-first-order kinetic analysis (with respect to catalyst) for the dehydrogenation of 1-phenyl ethanol at room temperature. (a) Change in absorbance with catalyst concentration variation. (b) Rate constant calculation. (c) Plot of k_{obs} vs change in catalyst concentration.

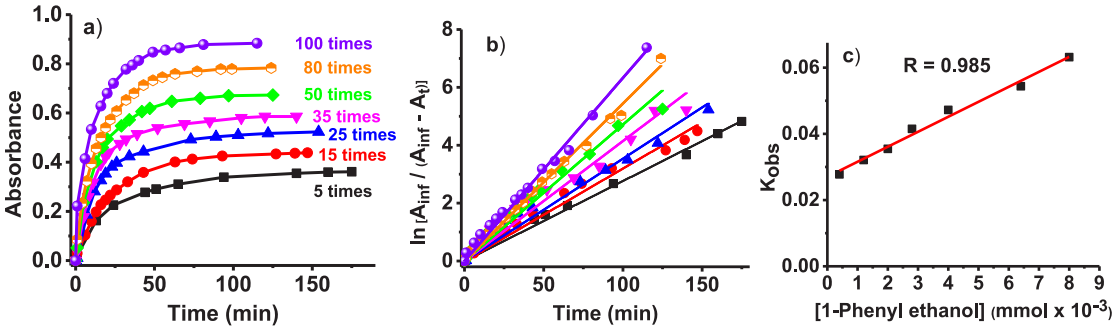

Figure 9. Pseudo-first-order kinetic analysis (with respect to substrate) for the dehydrogenation of 1-phenyl ethanol at room temperature. (a) Change in absorbance with substrate concentration variation. (b) Rate constant calculation. (c) Plot of k_{obs} vs change in substrate concentration.

showed a linear dependence on both catalyst and substrate concentration (Figures 8 and 9). A linear increase in the rate constant (k_{obs}) was observed upon increasing the catalyst loading over a range of 0.02−0.25 mol % with respect to the substrate (**15e**). A similar, linear rise of k_{obs} was also noticed when the concentration of the substrate (**15e**) was increased over the range of 5−100 equiv with respect to the catalyst (**1b**). Thus, the rate equation for the dehydrogenation of 1-phenyl ethanol (**15e**) can be expressed as rate = k[**1b**][1-phenylethanol]. The nonzero intercepts observed in the kinetic plots may be attributed to the KO^{t}Bu-catalyzed dehydrogenation of **15e**. Under the optimized conditions, in the presence of 0.1 equiv of base we observed ∼5% of conversion of **15e** to **18a**. The kinetic data also corroborates the fact that the catalyst and the substrate are bound together in the rate-determining step.

On the basis of the results obtained from the above control experiments and available literature, a plausible mechanism is proposed in Scheme 6. In the presence of zinc dust, the catalyst **1b** undergoes one-electron reduction to form the active catalyst [**1b**]$^-$ (**A**). Deprotonated alcohols or the saturated N-heterocycles then bind the active catalyst [**1b**]$^-$ to form the intermediate **B**. The Zn(II)-stabilized azo-anion radical, in the next step, abstracts a hydrogen atom from the α-carbon atom of the O-coordinated alcohols or the N-coordinated heterocycles resulting in the ketyl-type radical anion intermediate **C**. Under aerobic conditions, intermediate **C** undergoes a rapid one-electron transfer, and the desired aldehyde/N-heterocycle is produced, leaving behind the intermediate **D**. In the absence of experimental evidence, the aerial oxidation of **C** via the formation of superoxide anion is intuitive.[22,23] In fact, oxidation of **C** by an equivalent of **B′** can also not be ruled out. A second molecule of deprotonated alcohol or saturated N-heterocycle then coordinates the intermediate **D** to form the intermediate **E**. It is believed that the monoanionic azo-chromophore in **D** abstracts the hydrogen during deprotonation of the second molecule of the alcohol or saturated N-heterocycle.[16,22] Finally, aerial oxidation of **E** generates H_2O_2 and forms **B′**, which on one-electron reduction in the presence of the zinc-dust completes the catalytic cycle. Notably, the electrochemically generated two-electron reduced hydrazo-species in the presence of alcohol produces H_2O_2 upon exposure to air (see SI).

The formation of quinazolin-4(3*H*)-ones and quinazolines via dehydrogenative coupling reactions is believed to proceed via the base-mediated condensation of 2-aminobenzamides and 2-aminobenzylamines with the in situ formed aldehydes to form the corresponding cyclic aminals which upon further [**1b**]$^-$ catalyzed dehydrogenation produce the desired products (Scheme 6). On the other hand, the in situ-formed aldehydes undergo base-mediated cross-aldol type condensation with the ketones to form α, β-unsaturated ketones, which upon further cyclization affords the desired quinolines (Scheme 6).

CONCLUSION

In summary, our present work represents an exclusively ligand-centered redox-controlled approach for the dehydrogenation of a wide variety of N-heterocycles under air. Utilizing a Zn(II)-stabilized azo-anion radical complex as the catalyst, dehydrogenation reactions were achieved via one-electron HAT pathway where all the electron transfer events occur at the aryl-azo scaffold and the Zn(II) acts as a template. Overall, the catalysts used herein are bench-stable, easy-to-prepare, cheap, and show good efficiency during dehydrogenation and dehydrogenative coupling reactions yielding a variety of N-heterocycles in moderate to good isolated yields. The successful development of similar approaches utilizing the metal-stabilized organic radicals is expected to open up many

https://doi.org/10.1021/acscatal.1c00275
ACS Catal. 2021, 11, 7498−7512

Scheme 6. Plausible Mechanistic Pathway

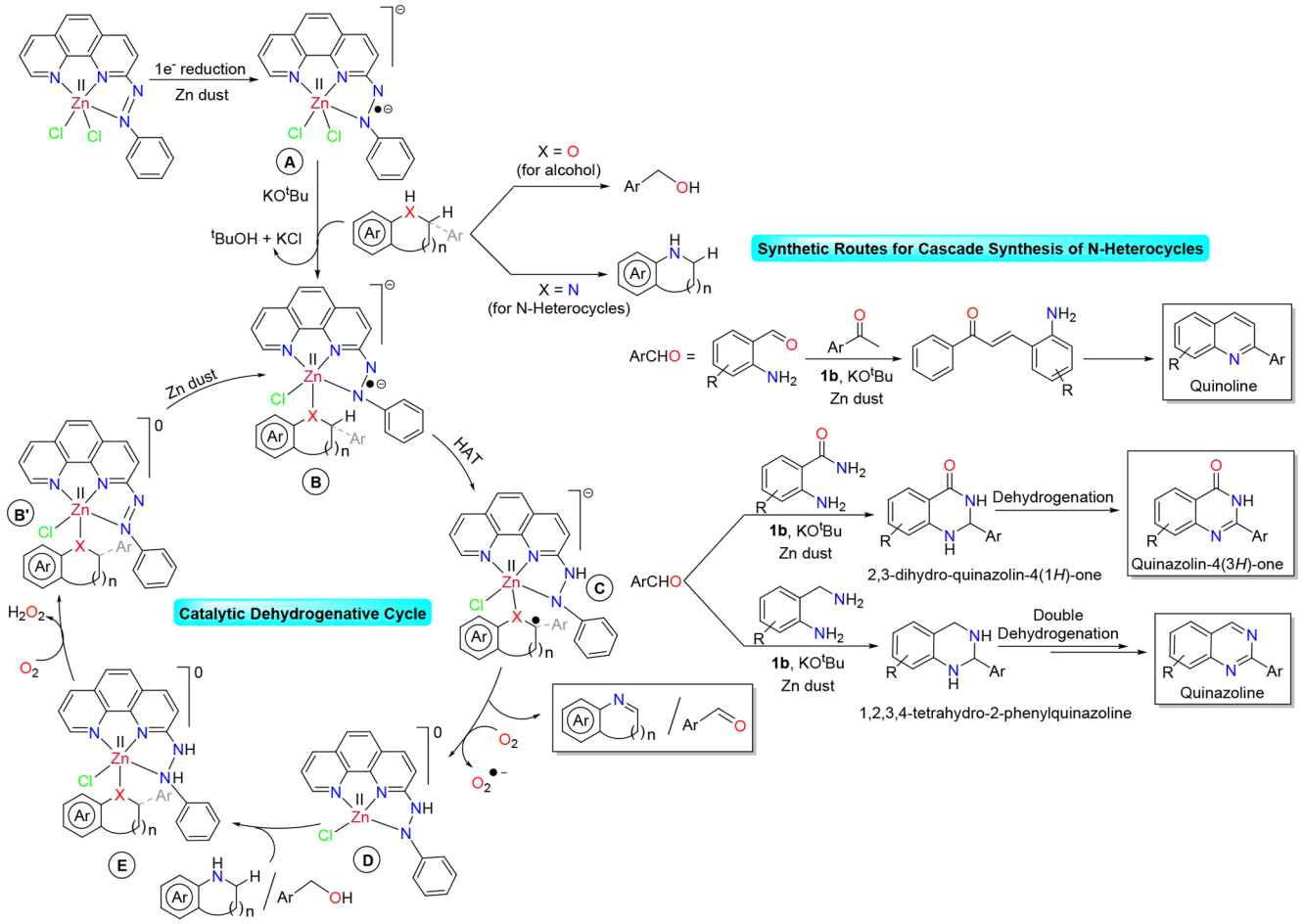

new chemical transformations, which usually require harsh reaction conditions or sometimes difficult to achieve following the classical synthetic routes.

EXPERIMENTAL SECTION

General Information. Toluene, xylene, and tetrahydrofuran (THF) used in the reactions were purified via distillation over sodium/benzophenone, maintaining an argon atmosphere, and were stored over 4 Å molecular sieves. All the other chemicals were commercially available and were used without further purification. Analytical TLC was done using Merck 60 F254 silica gel plate of 0.25 mm thickness, and column chromatography was performed with Merck 60 silica gel of 60−120 mesh. Bruker DPX-300 (300 MHz), Bruker DPX-400 (400 MHz), and Bruker DPX-500 (500 MHz) spectrometers were used for recording ^{1}H and ^{13}C NMR spectra. PerkinElmer 240C elemental analyzer was used for collecting microanalytical data (C, H, N). Q-TOF mass spectrometer (serial no. YA 263) was used for HRMS analysis. A PC-controlled AUT.MAC204 electrochemistry system was used for all electrochemical measurements. Cyclic voltammetry experiments were performed under a nitrogen atmosphere using an Ag/AgCl reference electrode, with a Pt-disk working electrode and a Pt-wire auxiliary electrode, in acetonitrile containing supporting electrolyte, 0.1 M $[Et_4N]ClO_4$, respectively. A Pt-wire-gauge was used as the working electrode during coulometry. EPR spectra in the X band were recorded with a JEOL JES-FA200 spectrometer. Gouy balance (Sherwood Scientific, Cambridge, U.K.) was used for room-temperature magnetic moment measurements. Unless otherwise mentioned, all the catalytic reactions were performed under air. ***Caution!*** *Perchlorates have to be handled with care and appropriate safety precautions.*

Synthesis of Azo-aromatic Ligands L^{1a,1b}.[16] First, 1.0 g of 2-amino-1,10-phenanthroline (5.122 mmol) was taken in a 250 mL round-bottom flask. Next, 1.0 equiv of nitrosobenzene was dissolved in 20 mL of toluene and 10.0 equiv of NaOH was dissolved in distilled water separately. Then the NaOH solution was added to the round-bottom flask containing 2-amino-1,10-phenanthroline followed by the addition of nitrosobenzene solution in toluene. The round-bottom flask was then fitted with a water condenser and allowed to stir at 80 °C for 12 h. After the completion of the reaction, the toluene layer of the reaction mixture was separated and concentrated under a vacuum. The pure ligand was isolated via silica gel column chromatography using toluene/dichloromethane mixture as eluent.

Synthesis of Dichloro-2-(phenyldiazenyl)-1,10-phenanthroline-Zn(II) Complex (1a). In an oven-dried round-bottom flask, 100 mg (0.314 mmol) of the ligand, **L^{1a}**, was taken, and 10.0 mL of ethanol was added. To it, 42.8 mg (0.314 mmol) of anhydrous $ZnCl_2$ was added. An instantaneous formation of orange color precipitate was observed. The reaction mixture was stirred for 4 h at room temperature. Once

https://doi.org/10.1021/acscatal.1c00275
ACS Catal. 2021, 11, 7498−7512

the reaction was complete, the whole reaction mixture was filtered, and the precipitate obtained was purified by fractional crystallization with dichloromethane/hexane (10:1) solvent mixture. Its yield and characterization data are as follows: Yield 93%. Color: Orange. UV/vis: $\lambda_{max/nm}(\varepsilon, M^{-1}cm^{-1})$, 231-(12,628), 278(7,114), 329(11,708), 390(6,349). IR (KBr cm^{-1}): 1620 (ν, C = N), 1420 (ν, N = N). ^1H NMR (400 MHz, $CDCl_3$+1drop CD_3OD): δ (ppm) = 9.34 (dd, J = 4.6, 1.6 Hz, 1H), 8.94 (d, J = 8.4 Hz, 1H), 8.73−8.69 (m, 3H), 8.58 (dd, J = 8.2, 1.2 Hz, 1H), 8.59−8.56 (m, 1H), 8.12 (s, 1H), 8.05−8.02 (m, 1H), 7.71−7.65 (m, 3H). Elemental Analysis: $C_{18}H_{12}Cl_2N_4Zn$: calcd: C, 51.40; H, 2.88; N, 13.32. Found: C, 51.32; H, 3.00; N, 13.43.

Synthesis of Dichloro-2-((4-chlorophenyl)diazenyl)-1,10-phenanthroline-Zn(II) Complex (1b). Catalyst **1b** was prepared following the same procedure as catalyst **1a**. Its yield and characterization data are as follows: Yield 94%. Color: Orange. UV/vis: $\lambda_{max/nm}(\varepsilon, M^{-1}cm^{-1})$, 238(10,988), 337(4,985), 396(9,128). IR (KBr cm^{-1}): 1580 (ν, C = N), 1420 (ν, N = N). ^1H NMR (400 MHz, $CDCl_3$+1drop CD_3OD): δ (ppm) = 9.30 (d, J = 3.6 Hz, 1H), 8.94 (d, J = 8.0 Hz, 1H), 8.70 (d, J = 8.4 Hz, 1H), 8.67 (d, J = 8.8 Hz, 2H), 8.59 (d, J = 8.0 Hz, 1H), 8.12 (s, 2H), 8.05−8.02 (m, 1H), 7.63 (d, J = 8.8 Hz, 2H). Elemental Analysis: $C_{18}H_{11}Cl_3N_4Zn$: calcd: C, 47.51; H, 2.44; N, 12.31. Found: C, 47.40; H, 2.56; N, 12.44.

General Procedure for Catalytic Dehydrogenative Synthesis of N-Heterocycles. A mixture of catalyst **1b**, KO^{t}Bu, Zn dust, and the respective N-heterocycles were added to a 50.0 mL round-bottom flask in optimum amounts. To it, 5.0 mL of toluene was added. The round-bottom flask containing the reaction mixture was then fitted with a water condenser and placed in an oil bath preheated at the required optimum temperature. The reaction was continued for the specified time for respective N-heterocycles under air. After the completion of the reaction, the resulting mixture was concentrated under a vacuum. The dehydrogenated N-heterocycles were isolated in pure form by column chromatography (silica gel). Eluent: petroleum ether/ethyl acetate.

General Procedure for One-Pot Cascade Synthesis of Quinazolin-4(3*H*)-ones. A mixture of catalyst **1b** (4.0 mol %), KO^{t}Bu (0.5 equiv), Zn dust (0.5 equiv), alcohol (1.1 mmol), and 2-aminobenzamide (1.0 mmol) were added to a 50.0 mL round-bottom flask. To it, 5.0 mL of toluene was added. The round-bottom flask containing the reaction mixture was then fitted with a water condenser and placed in an oil bath preheated at 100 °C. The reaction was continued for 16 h under air. After the completion of the reaction, the resulting mixture was concentrated under a vacuum. The product was isolated in pure form by column chromatography (silica gel). Eluent: petroleum ether/ethyl acetate (3:1).

General Procedure for One-Pot Cascade Synthesis of Quinazolines. A mixture of catalyst **1b** (5.0 mol %), KO^{t}Bu (0.5 equiv), Zn dust (0.5 equiv), alcohol (1.1 mmol), and 2-aminobenzylamine (1.0 mmol) was added to a 50.0 mL round-bottom flask. To it, 5.0 mL of toluene was added. The round-bottom flask containing the reaction mixture was then fitted with a water condenser and placed in an oil bath preheated at 100 °C. The reaction was continued for 16 h under air. After the completion of the reaction, the resulting mixture was concentrated under a vacuum. The product was isolated in pure form by column chromatography (silica gel). Eluent: petroleum ether/ethyl acetate (20:1).

General Procedure for One-Pot Cascade Synthesis of Quinolines. A mixture of catalyst **1b** (1.0 mol %), KO^{t}Bu (0.3 equiv), Zn dust (0.4 equiv), ketone (1.1 mmol), and 2-aminobenzylalcohol (1.0 mmol) was added to a 50.0 mL round-bottom flask. To it, 5.0 mL of toluene was added. The round-bottom flask containing the reaction mixture was then fitted with a water condenser and placed in an oil bath preheated at 90 °C. The reaction was continued for 10 h under air. After completion of the reaction, the resulting mixture was concentrated under a vacuum. The product was isolated in pure form by column chromatography (silica gel). Eluent: petroleum ether/ethyl acetate (20:1).

Detection of Hydrogen Peroxide during the Catalytic Reactions.[16] Production of H_2O_2 during catalytic dehydrogenation reactions was detected spectrophotometrically. The gradual formation of characteristic absorption band for I_3^- at 350 nm was monitored. 1-Phenylethanol (1.0 mmol), KO^{t}Bu (0.1 mmol), Zn-dust (0.5 equiv), and 2.0 mol % of catalyst **1b** were added in a 50 mL round-bottom flask containing a stir bar. To it, 5.0 mL of dry toluene was added and stirred at room temperature for 4 h. Then 5.0 mL of distilled water was added to the reaction mixture, and the resultant solution was extracted three times with dichloromethane. To stop further dehydrogenation of alcohol, the separated aqueous layer thus obtained was then acidified with H_2SO_4 to pH 2. A 10% KI solution and a few drops of 3.0% ammonium molybdate solution were added to it. The hydrogen peroxide generated during the catalytic cycle oxidizes I^- to I_2, which reacts with excess I^- to form I_3^- according to the following chemical reactions:

$$\text{(i) } H_2O_2 + 2I^- + 2H^+ \rightarrow 2H_2O + I_2\text{; (ii) } I_2(aq) + I^- \rightarrow I_3^-$$

Procedure for Kinetic Studies. To a 20.0 mL round-bottom flask, required amounts of 1-phenyl ethanol (**15e**), catalyst (**1b**), KO^{t}Bu (0.1 equiv), and zinc dust (0.5 equiv) were added under air. To this mixture, 8.0 mL of dry toluene was added, and the reaction mixture was stirred at room temperature under air. A 0.1 mL aliquot of the reaction mixture was taken from the round-bottom flask after a certain time interval, and the spectral changes were monitored at 290 nm with appropriate dilution.

X-ray Crystallography. We obtained single crystals of **1b**, suitable for X-ray diffraction, via slow evaporation of its solution in dichloromethane-hexane (10:1) solvent mixture. Single-crystal X-ray diffraction data of **1b** were collected with monochromated Mo Kα radiation (λ = 0.71073 Å) on a Bruker SMART Apex II diffractometer equipped with a CCD area detector. Data reduction was performed with SAINT-NT software package.[24] SADABS program was employed to apply multiscan absorption correction to all intensity data.[25] A combination of direct methods with subsequent difference Fourier syntheses were used to solve the crystal structure, and it was refined by full-matrix least-squares on F^2 using the SHELX-2013 suite.[26] An anisotropic treatment was given to the non-hydrogen atoms in all the cases. The crystal data, along with the refinement details, are shown in Table S1.

https://doi.org/10.1021/acscatal.1c00275
ACS Catal. 2021, 11, 7498−7512

Computational Details. Gaussian 09 program was used to perform all the DFT calculations.[27] B3LYP hybrid functional (G09/B3LYP) was used.[28] No geometric constraints were imposed during geometry optimizations. For Zn, the quasi-relativistic effective core pseudo potential proposed by Hay and Wadt, LANL2DZ pseudo potential,[29] and the corresponding optimized set of basis function has been employed. For carbon, hydrogen, nitrogen, and chlorine 6-31G* basis set[28] was used.

■ ASSOCIATED CONTENT

Supporting Information

The Supporting Information is available free of charge at https://pubs.acs.org/doi/10.1021/acscatal.1c00275.

ORTEP, FMOs, characterization data of all the synthesized compounds, copies of ^{1}H and ^{13}C NMR spectral data (PDF)

X-ray data for **1** (CIF)

■ AUTHOR INFORMATION

Corresponding Author

Nanda D. Paul − *Department of Chemistry, Indian Institute of Engineering Science and Technology, Howrah 711103, India;* orcid.org/0000-0002-8872-1413; Email: ndpaul@gmail.com, ndpaul2014@chem.iiests.ac.in

Authors

Siuli Das − *Department of Chemistry, Indian Institute of Engineering Science and Technology, Howrah 711103, India*

Rakesh Mondal − *Department of Chemistry, Indian Institute of Engineering Science and Technology, Howrah 711103, India*

Gargi Chakraborty − *Department of Chemistry, Indian Institute of Engineering Science and Technology, Howrah 711103, India*

Amit Kumar Guin − *Department of Chemistry, Indian Institute of Engineering Science and Technology, Howrah 711103, India*

Abhishek Das − *School of Chemical Sciences, Indian Association for the Cultivation of Science, Jadavpur, Kolkata 700032, India*

Complete contact information is available at: https://pubs.acs.org/10.1021/acscatal.1c00275

Author Contributions

S.D. did all the catalysis work. R.M., G.C., and A.K.G. participated during mechanistic investigations and NMR studies. A.D. did the EPR simulation. N.D.P. supervised and coordinated the project. N.D.P. and S.D. contributed during manuscript writing.

Notes

The authors declare no competing financial interest.

■ ACKNOWLEDGMENTS

The research was supported by DST, Govt. of India (Project CRG/2019/001737) and Department of Science & Technology and Biotechnology, Govt. of West Bengal (Project ST/P/S&T/15G-13/2019). S.D., G.C., and A.K.G. thank UGC, and R.M. thanks CSIR for fellowship support. Financial assistance from IIESTS is acknowledged. DST-sponsored SAIF, IIESTS is acknowledged for providing SCXRD, HRMS, and NMR facilities. We sincerely thank Prof. T. K. Paine for helpful discussion during EPR simulation. We sincerely thank Dr. C. Bhattacharya and Sangeeta Ghosh for coulometry experiment.

■ REFERENCES

(1) (a) Bowman, A. C.; Sproules, S.; Wieghardt, K. Electronic Structures of the $[V(^{t}bpy)_3]^{z}$ (z = 3+, 2+, 0, 1-) Electron Transfer Series. *Inorg. Chem.* **2012**, *51*, 3707−3717. (b) Surawatanawong, P.; Sproules, S.; Neese, F.; Wieghardt, K. Electronic Structures and Spectroscopy of the Electron Transfer Series $[Fe(NO)L_2]^{z}$ (z = 1+, 0, 1-, 2-,3-; L = Dithiolene). *Inorg. Chem.* **2011**, *50*, 12064−12074. (c) Bowman, A. C.; Milsmann, C.; Atienza, C. C. H.; Lobkovsky, E.; Wieghardt, K.; Chirik, P. J. Synthesis and Molecular and Electronic Structures of Reduced Bis(imino)pyridine Cobalt Dinitrogen Complexes: Ligand versus Metal Reduction. *J. Am. Chem. Soc.* **2010**, *132*, 1676−1684. (d) Ye, S.; Sarkar, B.; Lissner, F.; Schleid, Th; van Slageren, J.; Fiedler, J.; Kaim, W. Three-Spin System with a Twist: A Bis(semiquinonato)Copper Complex with a Nonplanar Configuration at the Copper(II) Center. *Angew. Chem., Int. Ed.* **2005**, *44*, 2103−2106. (e) Doslik, N.; Sixt, T.; Kaim, W. The First Structural Characterization of An Azoaromatic Radical Anion Stabilized by Dicopper(I) Coordination. *Angew. Chem., Int. Ed.* **1998**, *37*, 2403. (f) Paul, N. D.; Rana, U.; Goswami, S.; Mondal, T. K.; Goswami, S. Azo Anion Radical Complex of Rhodium As A Molecular Memory Switching Device: Isolation, Characterization, and Evaluation of Current-Voltage Characteristics. *J. Am. Chem. Soc.* **2012**, *134*, 6520−6523. (g) Paul, N. D.; Samanta, S.; Goswami, S. Redox Induced Electron Transfer in Doublet Azo-Anion Diradical Rhenium (II) Complexes. Characterization of Complete Electron Transfer Series. *Inorg. Chem.* **2010**, *49*, 2649−2655.

(2) (a) Broere, D. J. L.; Plessius, R.; van der Vlugt, J. I. New Avenues for Ligand-Mediated Processes-Expanding Metal Reactivity by the Use of Redox-Active Catechol, o-Aminophenol and *o*-Phenylenediamine Ligands. *Chem. Soc. Rev.* **2015**, *44*, 6886−6915. (b) Luca, O. R.; Crabtree, R. H. Redox Active Ligands in Catalysis. *Chem. Soc. Rev.* **2013**, *42*, 1440−1459. (c) Dzik, W. I.; van der Vlugt, J. I.; Reek, J. N. H.; de Bruin, B. Ligands that Store & Release Electrons during Catalysis. *Angew. Chem., Int. Ed.* **2011**, *50*, 3356−3358. (d) van Leest, N. P.; Epping, R. F. J.; van Vliet, K. M.; Lankelma, M.; van den Heuvel, E. J.; Heijtbrink, N.; Broersen, R.; de Bruin, B. Single-Electron Elementary Steps in Homogeneous Organometallic Catalysis. *Adv. Organomet. Chem.* **2018**, *70*, 71−180. (e) de Bruin, B.; Gualco, P.; Paul, N. D. Redox Non-Innocent Ligands. In *Ligand Design in Metal Chemistry*; John Wiley & Sons, Ltd: Chichester, U.K., 2016; pp 176−204. (f) Lyaskovskyy, V.; de Bruin, B. Redox Non-Innocent Ligands: Versatile New Tools to Control Catalytic Reactions. *ACS Catal.* **2012**, *2*, 270−279.

(3) (a) van Leest, N. P.; Tepaske, M. A.; Oudsen, J. -P. H.; Venderbosch, B.; Rietdijk, N. R.; Siegler, M. A.; Tromp, M.; van der Vlugt, J. I.; de Bruin, B. Ligand Redox Non-Innocence in $[Co^{III}(TAML)]^{0/-}$ Complexes Affects Nitrene Formation. *J. Am. Chem. Soc.* **2020**, *142*, 552−563. (b) van der Vlugt, J. I. Radical-Type Reactivity and Catalysis by Single-Electron Transfer to or from Redox-Active Ligands. *Chem. - Eur. J.* **2019**, *25*, 2651−2662.

(4) (a) Joannou, M. V.; Hoyt, J. M.; Chirik, P. J. Investigations into the Mechanism of Inter- and Intramolecular Iron-Catalyzed [2 + 2] Cycloaddition of Alkenes. *J. Am. Chem. Soc.* **2020**, *142*, 5314−5330. (b) Schmidt, V. A.; Kennedy, C. R.; Bezdek, M. J.; Chirik, P. J. Selective [1,4]-Hydrovinylation of 1,3-Dienes with Unactivated Olefins Enabled by Iron Diimine Catalysts. *J. Am. Chem. Soc.* **2018**, *140*, 3443−3453. (c) Bagh, B.; Broere, D. L. J.; Sinha, V.; Kuijpers, P. F.; van Leest, N. P.; de Bruin, B.; Demeshko, S.; Siegler, M. A.; van der Vlugt, J. I. Catalytic Synthesis of N-Heterocycles via Direct $C(sp^3)$-H Amination Using an Air-Stable Iron(III) Species with a Redox-Active Ligand. *J. Am. Chem. Soc.* **2017**, *139*, 5117−5124. (d) Broere, D. L. J.; de Bruin, B.; Reek, J. N. H.; Lutz, M.; Dechert, S.; van der Vlugt, J. I. Intramolecular Redox-Active Ligand-to-Substrate Single-Electron Transfer: Radical Reactivity with a Palladium(II) Complex. *J. Am. Chem. Soc.* **2014**, *136*, 11574−11577. (e) Sikari, R.; Sinha, S.; Das, S.; Saha, A.; Chakraborty, G.; Mondal, R.; Paul, N. D.

Achieving Nickel Catalyzed C-S Cross-Coupling under Mild Conditions Using Metal-Ligand Cooperativity. *J. Org. Chem.* **2019**, *84*, 4072−4085. (f) Sikari, R.; Sinha, S.; Chakraborty, G.; Das, S.; van Leest, N. P.; Paul, N. D. C-N Cross-Coupling Reactions Under Mild Conditions Using Singlet Di-Radical Nickel(II)-Complexes as Catalyst: N-Arylation and Quinazoline Synthesis. *Adv. Synth. Catal.* **2019**, *361*, 4342−4353. (g) Sikari, R.; Chakraborty, G.; Guin, A. K.; Paul, N. D. Nickel-Catalyzed [4 + 2] Annulation of Nitriles and Benzylamines by C-H/N-H Activation. *J. Org. Chem.* **2021**, *86*, 279−290.

(5) (a) Ringenberg, M. R.; Kokatam, S. L.; Heiden, Z. M.; Rauchfuss, T. B. Redox-Switched Oxidation of Dihydrogen Using a Non-Innocent Ligand. *J. Am. Chem. Soc.* **2008**, *130*, 788−789. (b) Lorkovic, I. M.; Duff, R. R., Jr; Wrighton, M. S. Use of the Redox-Active Ligand 1,1′-Bis(diphenylphosphino)cobaltocene To Reversibly Alter the Rate of the Rhodium(I)-Catalyzed Reduction and Isomerization of Ketones and Alkenes. *J. Am. Chem. Soc.* **1995**, *117*, 3617−3618.

(6) (a) Dobereiner, G. E.; Crabtree, R. H. Dehydrogenation as a Substrate-Activating Strategy in Homogeneous Transition-Metal Catalysis. *Chem. Rev.* **2010**, *110*, 681−703. (b) Choi, J.; Roy MacArthur, A. H.; Brookhart, M.; Goldman, A. S. Dehydrogenation and Related Reactions Catalyzed by Iridium Pincer Complexes. *Chem. Rev.* **2011**, *111*, 1761−1779.

(7) (a) Schwarz, D. E.; Cameron, T. M.; Hay, P. J.; Scott, B. L.; Tumas, W.; Thorn, D. L. Hydrogen Evolution from Organic "Hydrides. *Chem. Commun.* **2005**, 5919−5921. (b) Clot, E.; Eisenstein, O.; Crabtree, R. H. Computational Structure-Activity Relationships in H_2 Storage: How Placement of N Atoms Affects Release Temperatures in Organic Liquid Storage Materials. *Chem. Commun.* **2007**, 2231−2233.

(8) (a) Zhong, J.-J.; To, W.-P.; Liu, Y.; Lu, W.; Che, C.-M. Efficient Acceptorless Photo-Dehydrogenation of Alcohols and N-Heterocycles with Binuclear Platinum(II) Diphosphite Complexes. *Chem. Sci.* **2019**, *10*, 4883−4889. (b) Pawar, S. A.; Chand, A. N.; Kumar, A. V. Polydopamine: An Amine Oxidase Mimicking Sustainable Catalyst for the Synthesis of Nitrogen Heterocycles under Aqueous Conditions. *ACS Sustainable Chem. Eng.* **2019**, *7*, 8274−8286. (c) Bang, S. B.; Kim, J. Efficient Dehydrogenation of 1,2,3,4-Tetrahydroquinolines Mediated by Dialkyl Azodicarboxylates. *Synth. Commun.* **2018**, *48*, 1291−1298. (d) Kojima, M.; Kanai, M. Tris(pentafluorophenyl)-borane-Catalyzed Acceptorless Dehydrogenation of N-Heterocycles. *Angew. Chem., Int. Ed.* **2016**, *55*, 12224−12227. (e) Fujita, K. I.; Tanaka, Y.; Kobayashi, M.; Yamaguchi, R. Homogeneous Perdehydrogenation and Perhydrogenation of Fused Bicyclic N-Heterocycles Catalyzed by Iridium Complexes Bearing a Functional Bipyridonate Ligand. *J. Am. Chem. Soc.* **2014**, *136*, 4829−4832. (f) Yamaguchi, R.; Ikeda, C.; Takahashi, Y.; Fujita, K. I. Homogeneous Catalytic System for Reversible Dehydrogenation-Hydrogenation Reactions of Nitrogen Heterocycles with Reversible Interconversion of Catalytic Species. *J. Am. Chem. Soc.* **2009**, *131*, 8410−8412.

(9) (a) Iosub, A. V.; Stahl, S. S. Catalytic Aerobic Dehydrogenation of Nitrogen Heterocycles Using Heterogeneous Cobalt Oxide Supported on Nitrogen-Doped Carbon. *Org. Lett.* **2015**, *17*, 4404−4407. (b) Deraedt, C.; Ye, R.; Ralston, W. T.; Toste, F. D.; Somorjai, G. A. Dendrimer-Stabilized Metal Nanoparticles as Efficient Catalysts for Reversible Dehydrogenation/Hydrogenation of N-Heterocycles. *J. Am. Chem. Soc.* **2017**, *139*, 18084−18092. (c) Ainembabazi, D.; An, N.; Manayil, J. C.; Wilson, K.; Lee, A. F.; Voutchkova-Kostal, A. M. Acceptorless Amine Dehydrogenation and Transamination Using Pd-Doped Hydrotalcites. *ACS Catal.* **2019**, *9*, 1055−1065. (d) Ryabchuk, P.; Agapova, A.; Kreyenschulte, C.; Lund, H.; Junge, H.; Junge, K.; Beller, M. Heterogeneous Nickel-Catalysed Reversible, Acceptorless Dehydrogenation of N-Heterocycles for Hydrogen Storage. *Chem. Commun.* **2019**, *55*, 4969−4972. (e) Jaiswal, G.; Subaramanian, M.; Sahoo, M. K.; Balaraman, E. A Reusable Cobalt Catalyst for Reversible Acceptorless Dehydrogenation and Hydrogenation of N-Heterocycles. *ChemCatChem* **2019**, *11*, 2449−2457.

(10) (a) Yamaguchi, R.; Ikeda, C.; Takahashi, Y.; Fujita, K. I. Homogeneous Catalytic System for Reversible Dehydrogenation-Hydrogenation Reactions of Nitrogen Heterocycles with Reversible Interconversion of Catalytic Species. *J. Am. Chem. Soc.* **2009**, *131*, 8410−8412. (b) Wu, J.; Talwar, D.; Johnston, S.; Yan, M.; Xiao, J. Acceptorless Dehydrogenation of Nitrogen Heterocycles with a Versatile Iridium Catalyst. *Angew. Chem. Angew. Chem., Int. Ed.* **2013**, *52*, 6983−6987. (c) Yao, W.; Zhang, Y.; Jia, X.; Huang, Z. Selective Catalytic Transfer Dehydrogenation of Alkanes and Heterocycles by an Iridium Pincer Complex. *Angew. Chem., Int. Ed.* **2014**, *53*, 1390−1394. (d) Manas, M. G.; Sharninghausen, L. S.; Lin, E.; Crabtree, R. H. Iridium Catalyzed Reversible Dehydrogenation -Hydrogenation of Quinoline Derivatives under Mild Conditions. *J. Organomet. Chem.* **2015**, *792*, 184−189. (e) Vivancos, Á.; Beller, M.; Albrecht, M. NHC-Based Iridium Catalysts for Hydrogenation and Dehydrogenation of N-Heteroarenes in Water under Mild Conditions. *ACS Catal.* **2018**, *8*, 17−21. (f) Wang, Z.; Tonks, I.; Belli, J.; Jensen, C. M. Dehydrogenation of N-ethyl Perhydrocarbazole Catalyzed by PCP Pincer Iridium Complexes: Evaluation of a Homogenous Hydrogen Storage System. *J. Organomet. Chem.* **2009**, *694*, 2854−2857. (g) Wang, S.; Huang, H.; Bruneau, C.; Fischmeister, C. Iridium-Catalyzed Hydrogenation and Dehydrogenation of N-Heterocycles in Water under Mild Conditions. *ChemSusChem* **2019**, *12*, 2350−2354.

(11) (a) Chakraborty, S.; Brennessel, W. W.; Jones, W. D. A Molecular Iron Catalyst for the Acceptorless Dehydrogenation and Hydrogenation of N-Heterocycles. *J. Am. Chem. Soc.* **2014**, *136*, 8564−8567. (b) Xu, R.; Chakraborty, S.; Yuan, H.; Jones, W. D. Acceptorless, Reversible Dehydrogenation and Hydrogenation of N-Heterocycles with a Cobalt Pincer Catalyst. *ACS Catal.* **2015**, *5*, 6350−6354.

(12) (a) Wendlandt, A. E.; Stahl, S. S. Bioinspired Aerobic Oxidation of Secondary Amines and Nitrogen Heterocycles with a Bifunctional Quinone Catalyst. *J. Am. Chem. Soc.* **2014**, *136*, 506−512. (b) Wendlandt, A. E.; Stahl, S. S. Modular o-Quinone Catalyst System for Dehydrogenation of Tetrahydroquinolines under Ambient Conditions. *J. Am. Chem. Soc.* **2014**, *136*, 11910−11913.

(13) (a) Alig, L.; Fritz, M.; Schneider, S. First-Row Transition Metal (De)Hydrogenation Catalysis Based On Functional Pincer Ligands. *Chem. Rev.* **2019**, *119*, 2681−2751. (b) Crabtree, R. H. Homogeneous Transition Metal Catalysis of Acceptorless Dehydrogenative Alcohol Oxidation: Applications in Hydrogen Storage and to Heterocycle Synthesis. *Chem. Rev.* **2017**, *117*, 9228−9246. (c) Mukherjee, A.; Milstein, D. Homogeneous Catalysis by Cobalt and Manganese Pincer Complexes. *ACS Catal.* **2018**, *8*, 11435−11469.

(14) (a) Yang, L.; Powell, D. R.; Houser, R. P. Structural Variation in Copper(I) Complexes with Pyridylmethylamide Ligands: Structural Analysis with A New Four-Coordinate Geometry Index, τ_4. *Dalton Trans.* **2007**, 955−964. (b) Addison, A. W.; Rao, T. N.; Reedijk, J.; van Rijn, J.; Verschoor, G. C. Synthesis, Structure, and Spectroscopic Properties of Copper(11) Compounds Containing Nitrogen-Sulphur Donor Ligands; the Crystal and Molecular Structure of Aqua[l,7-bis(N-methylbenzimidazol-2′-yl)-2,6-dithiaheptane]copper(ii) Perchlorate. *J. Chem. Soc., Dalton Trans.* **1984**, 1349−1356.

(15) Das, S.; Sinha, S.; Jash, U.; Sikari, R.; Saha, A.; Barman, S. K.; Brandão, P.; Paul, N. D. Redox-Induced Interconversion and Ligand-Centered Hemilability in Ni(II) Complexes of Redox-Noninnocent Azo-Aromatic Pincers. *Inorg. Chem.* **2018**, *57*, 5830−5841.

(16) Sinha, S.; Das, S.; Sikari, R.; Parua, S.; Brandaŏ, P.; Demeshko, S.; Meyer, F.; Paul, N. D. Redox Noninnocent Azo-Aromatic Pincers and Their Iron Complexes. Isolation, Characterization, and Catalytic Alcohol Oxidation. *Inorg. Chem.* **2017**, *56*, 14084−14100.

(17) (a) Luo, J.; Rauch, M.; Avram, L.; Diskin-Posner, Y.; Shmul, G.; Ben-David, Y.; Milstein, D. Formation of Thioesters by Dehydrogenative Coupling of Thiols and Alcohols with H_2 Evolution. *Nat. Catal* **2020**, *3*, 887−892. (b) Luque-Urrutia, J. A.; Sola, M.; Milstein, D.; Poater, A. Mechanism of the Manganese-Pincer Catalyzed Acceptorless Dehydrogenative Coupling of Nitriles and Alcohols. *J. Am. Chem. Soc.* **2019**, *141*, 2398−2403. (c) Daw, P.; Kumar, A.; Espinosa-

https://doi.org/10.1021/acscatal.1c00275
ACS Catal. 2021, 11, 7498−7512

Jalapa, N. A.; Diskin-Posner, Y.; Ben-David, Y.; Milstein, D. Synthesis of Pyrazines and Quinoxalines via Acceptorless Dehydrogenative Coupling Routes Catalyzed by Manganese Pincer Complexes. *ACS Catal.* **2018**, *8*, 7734−7741. (d) Daw, P.; Ben-David, Y.; Milstein, D. Direct Synthesis of Benzimidazoles by Dehydrogenative Coupling of Aromatic Diamines and Alcohols Catalyzed by Cobalt. *ACS Catal.* **2017**, *7*, 7456−7460. (e) Deraedt, C.; Ye, R.; Ralston, W. T.; Toste, F. D.; Somorjai, G. A. Dendrimer-Stabilized Metal Nanoparticles as Efficient Catalysts for Reversible Dehydrogenation/Hydrogenation of N-Heterocycles. *J. Am. Chem. Soc.* **2017**, *139*, 18084−18092. (f) Jana, A.; Das, K.; Kundu, A.; Thorve, P. R.; Adhikari, D.; Maji, B. A Phosphine-Free Manganese Catalyst Enables Stereoselective Synthesis of (1 + n) Membered Cycloalkanes from Methyl Ketones and 1,*n*-Diols. *ACS Catal.* **2020**, *10*, 2615−2626.

(18) (a) Liang, Y.; Tan, Z.; Jiang, H.; Zhu, Z.; Zhang, M. Copper-Catalyzed Oxidative Multicomponent Annulation Reaction for Direct Synthesis of Quinazolinones via an Imine-Protection Strategy. *Org. Lett.* **2019**, *21*, 4725−4728. (b) Parua, S.; Das, S.; Sikari, R.; Sinha, S.; Paul, N. D. One-Pot Cascade Synthesis of Quinazolin-4(3*H*)-ones via Nickel-Catalyzed Dehydrogenative Coupling of *o*-Aminobenzamides with Alcohols. *J. Org. Chem.* **2017**, *82*, 7165−7175.

(19) (a) Mondal, A.; Sahoo, M. K.; Subaramanian, M.; Balaraman, E. Manganese(I)-Catalyzed Sustainable Synthesis of Quinoxaline and Quinazoline Derivatives with the Liberation of Dihydrogen. *J. Org. Chem.* **2020**, *85*, 7181−7191. (b) Das, K.; Mondal, A.; Pal, D.; Srimani, D. Quinazoline and 2-Aminoquinoline via Dehydrogenative Coupling of 2-Aminobenzyl Alcohol and Nitrile Catalyzed by Phosphine-Free Manganese Pincer Complex. *Org. Lett.* **2019**, *21*, 3223−3227.

(20) (a) Das, S.; Sinha, S.; Samanta, D.; Mondal, R.; Chakraborty, G.; Brandaõ, P.; Paul, N. D. Metal-Ligand Cooperative Approach To Achieve Dehydrogenative Functionalization of Alcohols to Quinolines and Quinazolin-4(3*H*)-ones under Mild Aerobic Conditions. *J. Org. Chem.* **2019**, *84*, 10160−10171. (b) Parua, S.; Sikari, R.; Sinha, S.; Das, S.; Chakraborty, G.; Paul, N. D. A Nickel Catalyzed Acceptorless Dehydrogenative Approach to Quinolines. *Org. Biomol. Chem.* **2018**, *16*, 274−284. (c) Mastalir, M.; Glatz, M.; Pittenauer, E.; Allmaier, G.; Kirchner, K. Sustainable Synthesis of Quinolines and Pyrimidines Catalyzed by Manganese PNP Pincer Complexes. *J. Am. Chem. Soc.* **2016**, *138*, 15543−15546.

(21) (a) Ray, R.; Chandra, S.; Maiti, D.; Lahiri, G. K. Simple and Efficient Ruthenium-Catalyzed Oxidation of Primary Alcohols with Molecular Oxygen. *Chem. - Eur. J.* **2016**, *22*, 8814−8822. (b) Chakraborty, G.; Sikari, R.; Das, S.; Mondal, R.; Sinha, S.; Banerjee, S.; Paul, N. D. Dehydrogenative Synthesis of Quinolines, 2-Aminoquinolines, and Quinazolines Using Singlet Diradical Ni(II)-Catalysts. *J. Org. Chem.* **2019**, *84*, 2626−2641. (c) Ma, Y.; Du, Z.; Liu, J.; Xia, F.; Xu, J. Selective Oxidative C-C Bond Cleavage of a Lignin Model Compound in the Presence of Acetic Acid with a Vanadium Catalyst. *Green Chem.* **2015**, *17*, 4968.

(22) Sengupta, D.; Bhattacharjee, R.; Pramanick, R.; Rath, S. P.; Saha Chowdhury, N.; Datta, A.; Goswami, S. Exclusively Ligand-Mediated Catalytic Dehydrogenation of Alcohols. *Inorg. Chem.* **2016**, *55*, 9602−9610.

(23) Pramanick, R.; Bhattacharjee, R.; Sengupta, D.; Datta, A.; Goswami, S. An Azoaromatic Ligand as Four Electron Four Proton Reservoir: Catalytic Dehydrogenation of Alcohols by Its Zinc(II) Complex. *Inorg. Chem.* **2018**, *57*, 6816−6824.

(24) Bruker. *SAINT-plus*; Bruker AXS Inc.: Madison, WI, 2007.

(25) Sheldrick, G. M. *SADABS*; University of Göttingen: Germany, 1996.

(26) Sheldrick, G. M. *Acta Crystallogr., Sect. A: Found. Crystallogr.* **2008**, *64*, 112−122.

(27) Frisch, M. J.; Trucks, G. W.; Schlegel, H. B.; Scuseria, G. E.; Robb, M. A.; Cheeseman, J. R.; Scalmani, G.; Barone, V.; Mennucci, B.; Petersson, G. A.; Nakatsuji, H.; Caricato, M.; Li, X.; Hratchian, H. P.; Izmaylov, A. F.; Bloino, J.; Zheng, G.; Sonnenberg, J. L.; Hada, M.; Ehara, M.; Toyota, K.; Fukuda, R.; Hasegawa, J.; Ishida, M.; Nakajima, T.; Honda, Y.; Kitao, O.; Nakai, H.; Vreven, T.; Montgomery, J. A., Jr; Peralta, J. E.; Ogliaro, F.; Bearpark, M.; Heyd, J. J.; Brothers, E.; Kudin, K. N.; Staroverov, V. N.; Kobayashi, R.; Normand, J.; Raghavachari, K.; Rendell, A.; Burant, J. C.; Iyengar, S. S.; Tomasi, J.; Cossi, M.; Rega, N.; Millam, N. J.; Klene, M.; Knox, J. E.; Cross, J. B.; Bakken, V.; Adamo, C.; Jaramillo, J.; Gomperts, R.; Stratmann, R. E.; Yazyev, O.; Austin, A. J.; Cammi, R.; Pomelli, C.; Ochterski, J. W.; Martin, R. L.; Morokuma, K.; Zakrzewski, V. G.; Voth, G. A.; Salvador, P.; Dannenberg, J. J.; Dapprich, S.; Daniels, A. D.; Farkas, Ö.; Foresman, J. B.; Ortiz, J. V.; Cioslowski, J.; Fox, D. J. *Gaussian 09*, revision B.01; Gaussian, Inc.: Wallingford, CT, 2010.

(28) Stephens, P. J.; Devlin, F. J.; Chabalowski, C. F.; Frisch, M. J. Ab Initio Calculation of Vibrational Absorption and Circular Dichroism Spectra Using Density Functional Force Fields. *J. Phys. Chem.* **1994**, *98*, 11623−11627.

(29) Hay, P. J.; Wadt, W. R. Ab initio effective core potentials for molecular calculations. Potentials for the transition metal atoms Sc to Hg. *J. Chem. Phys.* **1985**, *82*, 270−283.

https://doi.org/10.1021/acscatal.1c00275
ACS Catal. 2021, 11, 7498−7512